**Short title:** Portable LiDAR and 3D field phenotyping in wheat

# Large-scale field phenotyping using backpack LiDAR and CropQuant-3D to measure structural variation in wheat

**Authors**

Yulei Zhu[1+], 2018112022@njau.edu.cn

Gang Sun[1], 2018101176@njau.edu.cn

Guohui Ding[1], 2018201009@njau.edu.cn, orcid: 0000-0001-5498-6838

Jie Zhou[1], 2018812070@njau.edu.cn, orcid: 0000-0001-7162-4791

Mingxing Wen[1,2], 2017201063@njau.edu.cn

Shichao Jin[1], jschaon@njau.edu.cn, orcid: 0000-0003-1150-336X

Qiang Zhao[3], zqiang@ncgr.ac.cn, orcid: 0000-0002-8372-4463

Joshua Colmer[4], Josh.Colmer@earlham.ac.uk, orcid: 0000-0002-0511-685X

Yanfeng Ding[1], dingyf@njau.edu.cn

Eric S. Ober[5], Eric.Ober@niab.com, orcid: 0000-0002-4832-5897

Ji Zhou[1,5*], Ji.Zhou@njau.edu.cn, Ji.Zhou@NIAB.com, orcid: 0000-0002-5752-5524

[1]State Key Laboratory of Crop Genetics & Germplasm Enhancement, College of Engineering, College of Agriculture, Plant Phenomics Research Center, Academy for Advanced Interdisciplinary Studies, Jiangsu Collaborative Innovation Center for Modern Crop Production Co-sponsored by Province and Ministry, Nanjing Agricultural University, Nanjing 210095, China; [2]Zhenjiang Institute of Agricultural Science, Jurong 212400, China; [3]National Center for Gene Research, CAS Center for Excellence in Molecular Plant Sciences, Chinese Academy of Sciences, Shanghai 200233, China; [4]Earlham Institute, Norwich Research Park, Norwich NR4 7UH, UK; [5]Cambridge Crop Research, National Institute of Agricultural Botany (NIAB), Cambridge CB3 0LE, UK

**Corresponding author**

Ji Zhou

Email: Ji.Zhou@NJAU.edu.cn or Ji.Zhou@NIAB.com

**One-sentence summary:**

CropQuant-3D and backpack LiDAR enable large-scale field phenotyping and 3D trait analysis to quantify structural responses to different nitrogen treatments in wheat.

**Author contributions**

JZ and EO wrote the manuscript with inputs from YLZ, SCJ, QZ and JC. JZ, YLZ and GS designed the 3D phenotypic analysis algorithms. YLZ, GS and JieZ implemented the software under JZ's supervision. GHD and MXW performed the field wheat experiments under JZ and YFD's supervision. SCJ provided LiDAR expertise. JZ, YLZ and JieZ optimised the algorithms and tested the software. JZ, QZ and JC performed the data analysis. All authors read and approved the final manuscript.

**Funding**

The wheat field experiments are supported by the National Natural Science Foundation of China (32070400 to JZ). GHD and the field team were supported by Natural Science Foundation of Jiangsu Province (BK20191311 to JZ). JZ was partially funded by the United Kingdom Research and Innovation's (UKRI) Biotechnology and Biological Sciences Research Council (BBSRC) Designing Future Wheat Strategic Programme (BB/P016855/1). YFD were supported by Jiangsu Collaborative Innovation Center for Modern Crop Production. QZ was supported by Chinese Academy of Sciences (XDA24020205 to QZ). JC was supported by the BBSRC's National Productivity Investment Fund CASE Award, hosted at Norwich Research Park Biosciences Doctoral Training Partnership (BB/M011216/1). JieZ, YLZ and GS were supported by the Fundamental Research Funds for the Central Universities in China (JCQY201902).

**Abstract**

Plant phenomics bridges the gap between traits of agricultural importance and genomic information. Limitations of current field-based phenotyping solutions include mobility, affordability, throughput, accuracy, scalability and the ability to analyse big data collected. Here, we present a large-scale phenotyping solution that combines a commercial backpack LiDAR device and our analytic software, CropQuant-3D, which have been applied jointly to phenotype wheat (*Triticum aestivum*) and associated 3D trait analysis. The use of LiDAR can acquire millions of 3D points to represent spatial features of crops, and CropQuant-3D can extract meaningful traits from large, complex point clouds. In a case study examining the response of wheat varieties to three different levels of nitrogen fertilisation in field experiments, the combined solution differentiated significant genotype and treatment effects on crop growth and structural variation in canopy, with strong correlations with manual measurements. Hence, we demonstrate that this system could consistently perform 3D trait analysis at a larger scale and more quickly than heretofore possible and addresses challenges in mobility, throughput, and scalability. To ensure our work could reach non-expert users, we developed an open-source graphical user interface for CropQuant-3D. We therefore believe that the combined system is easy-to-use and could be used as a reliable research tool in multi-location phenotyping for both crop research and breeding. Furthermore, together with the fast maturity of LiDAR technologies, the system has the potential for further development in accuracy and affordability, contributing to the resolution of the phenotyping bottleneck and exploiting available genomic resources more effectively.

**Keywords**

Field phenotyping, backpack LiDAR, 3D trait analysis, nitrogen responses, wheat

## Introduction

With the rising world population, crop production needs to double by 2050 (UN Food & Agriculture Organization, 2009). To address this growing challenge of global food security, it is important to identify plants with desired traits to improve yield, resource use efficiency, quality, stress resistance and adaptation, and with a smaller environmental footprint (Powlson et al., 2014; Zhang et al., 2018; Swarbreck et al., 2019). Furthermore, the stability of the selected traits must be verified in the field over multiple seasons and locations (Sadras and Slafer, 2012; Griffiths et al., 2015; Reynolds and Langridge, 2016). For example, quantitative measurements of yield-related traits such as plant height, growth rate, canopy coverage and spikes per unit area can be used to indicate and explain variations in yield stability in different environments (Sadras and Richards, 2014; Valluru et al., 2017; Furbank et al., 2019). In recent years, the cost of genotyping has decreased dramatically, allowing genetic analysis of large populations (Cobb et al., 2013; Crain et al., 2016). However, field phenotyping on a large scale under realistic field conditions remains the bottleneck in genotype-phenotype association studies for crop improvement (Furbank and Tester, 2011; Yang et al., 2020). Both large-scale data acquisition and analysis of multiple traits at different time points and trial locations are still challenging, but often it is the meaningful phenotypic information most needed by breeders and crop researchers (Fiorani and Schurr, 2013; Tardieu et al., 2017; Furbank et al., 2019).

To relieve this bottleneck and address challenges in field phenotyping, much attention has been placed upon the applications of remote sensing, internet of things (IoT), robotics, computer vision, and machine learning, resulting in a rapid technical progress in recent years (Pieruschka and Schurr, 2019; Zhao et al., 2019; Yang et al., 2020). A range of solutions have been developed, including the use of unmanned aerial vehicles (UAVs) and manned light aircraft for studying performance-related traits across fields (Bauer et al., 2019; Holman et al., 2019; Harkel et al., 2020); stationary gantry systems for deep phenotyping in fixed areas (Vadez et al., 2015; Kirchgessner et al., 2017; Virlet et al., 2017; Burnette et al., 2018); ground-based vehicles equipped with integrated sensor arrays to study canopy-related traits (Deery et al., 2014; Barker et al., 2016; Jimenez-Berni et al., 2018); hand-held or distributed sensing devices to measure various phenotypes during key growth stages (Hirafuji and Yoichi, 2011; Crain et al., 2016; Zhou et al., 2017b; Reynolds et al., 2019a). These methods possess

diverse advantages and disadvantages concerning throughput, accuracy, mobility, affordability, scalability and, more importantly, biological relevance (Fritsche-Neto and Borém, 2015; Furbank et al., 2019; Pieruschka and Schurr, 2019; Reynolds et al., 2019b; Roitsch et al., 2019). The selection of a phenotyping approach is naturally depending on the nature of the research question; but despite the rapid methodological progress, gaps in large-scale field solutions remain.

Among recent field-based solutions, Light Detection and Ranging (LiDAR) has attracted much attention as it provides information on plant morphological and structural features that are difficult or costly to quantify through traditional approaches (Lin, 2015; Stovall et al., 2017). As an active remote sensing technique, LiDAR computes the distance from laser scanners to a given target using pulsed laser beams, through which three-dimensional (3D) geometric features of the targeted object can be recorded in point cloud datasets (Arnó et al., 2013). LiDAR-based tools have been successful in overcoming issues related to natural illumination and occlusion, which have been problematic for many field-based methods (Sun et al., 2018; Jin et al., 2019). Although point clouds produced by LiDAR can be subject to noise and imbalanced densities (Bucksch et al., 2009), recently developed open-source analysis libraries such as WhiteboxTools (Lindsay, 2016) and Open3D (Zhou et al., 2018) can be utilised to conduct point clouds processing. However, these libraries were developed for generic 3D analysis, which requires experienced developers with a computer vision background to develop tailored solutions to analyse specific LiDAR data, limiting their use by plant researchers.

LiDAR devices can be roughly classified into three types: airborne, fixed terrestrial and mobile (Hosoi and Omasa, 2009; Lin, 2015). Plant characters that have been estimated include: crop height, biomass, and canopy structure (Omasa et al., 2007; Naito et al., 2017; Harkel et al., 2020); leaf number, shape, and the plant capacity to intercept solar radiation (Sun et al., 2018; Jin et al., 2019); and grain yield (Jimenez-Berni et al., 2018; Li et al., 2020b). LiDAR-generated point clouds have also been used to improve parameterisation of crop models, enabling *in silico* testing to optimise trait combinations in breeding and crop growth simulation (Reynolds and Langridge, 2016; Wang et al., 2017; Walter et al., 2019). In comparison with alternative approaches that can also record 3D plant traits such as Structure from Motion (SfM) (Duan et al., 2016), time-of-flight (Paulus, 2019), micro-computed tomography (Wu et al., 2019), and photogrammetry techniques (An et al., 2016; Holman et

al., 2016), LiDAR provides a more reliable solution in scalability and accuracy for high-throughput field studies.

Despite these advantages, there are several problems associated with current LiDAR techniques in field phenotyping. Airborne LiDAR (Li et al., 2015; Harkel et al., 2020) typically requires larger multi-rotor UAVs with sufficient payload capacity (normally >5 kg), which requires special trained pilot and local aviation authority's clearance, adding to hardware and operating costs. Also, big drones generate strong downdraft that disrupts canopies when flying them at low altitudes to acquire high-resolution imagery. Fixed terrestrial LiDAR (Omasa et al., 2007; Stovall et al., 2017; Guo et al., 2018), on the other hand, is placed closer to plants and can generate high-resolution models. Nevertheless, this type of system requires more time to set up, limiting its applications in large-scale phenotyping. Mobile LiDAR (Arnó et al., 2013; Araus and Cairns, 2014; Deery et al., 2014; Jimenez-Berni et al., 2018; Deery et al., 2020) includes handheld, backpack, and devices mounted on specialised vehicles (e.g. Phenomobile), which can cover large trial areas. The main drawbacks of vehicle-mounted LiDAR are the costs of purchasing hardware, operating and maintenance, as well as the ability to access agricultural fields with difficult conditions or rugged terrain. Handheld LiDAR devices are lightweight and easy-to-use, but usually are equipped with low-cost laser sensors, limiting their capability to carry out high-quality and large-scale 3D mapping (Hyyppä et al., 2020; Jin et al., 2021).

The backpack LiDAR (Masiero et al., 2018; Hyyppä et al., 2020; Su et al., 2020) has been applied successfully to forestry studies and land surveillance in recent years, showing promise for field-based crop research. Compare with other LiDAR systems, it has good mobility, relatively lightweight (normally around 10 kg), and is highly integrated in hardware, which means that it is easy to operate and maintain. Because the laser scanner can be used in close proximity to plants (< 3 m), it can generate high-quality 3D models with up to 10 mm precision with high-end laser sensors. Depending on the laser scanner equipped, backpack LiDAR system could have an effective scan range of over 200 m, useful for phenotyping in forestry or orchard plantations, as well as large experimental areas for plants. Backpack LiDAR also provides an accurate spatial positioning system (i.e. a global navigation satellite system, GNSS), customised for field mapping at walking speed to enable an

accurate 3D reconstruction (Masiero et al., 2018). As LiDAR technology has been maturing rapidly in recent years, it is expected that costs will decrease and this type of equipment could become more accessible for the research community (Guo et al., 2018; Panjvani et al., 2019; Jin et al., 2021). Still, the analytic software for LiDAR-based technologies is as important as the hardware. One limitation of many LiDAR-based mapping systems is the lack of widely available, open analytical software solutions that can extract biologically relevant information from the large point cloud data (Lin, 2015; Zhao et al., 2019; Yang et al., 2020), preventing non-expert users from taking advantage of this technology for rapidly modelling crop structural features and mining phenotypic information to study spatial and temporal changes (Ubbens et al., 2018; Panjvani et al., 2019; Ward et al., 2019).

Here, we introduce an integrated solution that combines a backpack LiDAR device with open-source analytic software called CropQuant-3D for processing large-scale field phenotyping and 3D trait analysis. The software employs 2D/3D image analysis algorithms and Discrete Fourier Transform to derive plot-based measurements of key performance-related traits such as crop height and structural variation in canopy. We developed a range of technical applications to integrate the backpack LiDAR and CropQuant-3D into field-based phenotyping, including a large-scale mapping protocol for cereal crops, the quick quality assessment of collected datasets at different sites, and a comprehensive analysis pipeline. In a case study of wheat (*Triticum aestivum*), we describe the integrated solution to quantify varietal responses to three levels of nitrogen (N) fertilisation of eleven Chinese winter wheat varieties selected from the 'Zhenmai' and 'Ningmai' populations. By combining 3D trait analysis and manual key yield components, we also produced a performance matrix to rank and evaluate genotypic differences in N responses for the examined varieties, resulting in the classification of four N response types. To ensure that our work could reach the broader research community, we have developed a graphical user interface (GUI) for CropQuant-3D so that non-expert users could use the software easily. Furthermore, we expanded the software package to analyse point clouds generated from other sources such as gantry-mounted LiDAR and UAV-SfM photogrammetry. We uploaded the CropQuant-3D software (in EXE format), executable analysis source code (in Jupyter notebooks), and testing datasets to our GitHub repository, which are openly available for the plant research community. Hence, we believe that the integrated solution presented

here is capable of addressing challenges in mobility, throughput, scalability and enabling us to analyse big LiDAR-collected 3D point cloud data, which is likely to help plant researchers bridge the gap between traits of agricultural importance and available genetic resources for crop improvement.

## Results

*In-field mapping protocol using the backpack LiDAR*

Because limited research has been conducted on the use of backpack LiDAR in field phenotyping, we therefore developed a range of technical applications to utilise the device in the field, including the optimal distance to map cereal crops, the design of mapping routes and angles, the quick assessment of the data quality, and the calibration method at different sites. For example, a grid-style mapping approach was designed to routinely map the large field trial in this study (red arrows in **Fig. 1a)**. We first recorded the 3D geo-coordinates of the trial area using a real-time kinematic (RTK) base station, which logged satellite-based positions with ± 5 mm error range in 3D (**Fig. 1b**). Then, a LiDAR operator walked around the perimeter of each N treatment block in the field to map the entire experiment from different angles. Due to the scan range of the LiDAR device, we did not need to walk around each individual plot, saving significant time in operation. On average, it took the LiDAR operator 20-25 minutes to map an experiment field of 0.5-ha, equivalent to a mapping speed of around 1.2 ha per hour. To study canopy structural responses to different N, we focused on the growth stages between heading (GS51-59) and grain filling (GS71-89) when canopy was largely established (Zadocks et al., 1974).

*Data pre-processing to generate 3D point clouds*

According to standard practice in processing 3D points (Kachamba et al., 2016; Duan et al., 2017; Sun et al., 2018), we used the bundled pre-processing software to generate GPS-tagged 3D point clouds collected by the LiDAR (**Fig. 1c**). The bundled software we used are: MMProcess to build up a 3D mapping project, AERO-office to define the mapping path, and GrafNav to associate RTK GPS signals with the path. To select, visualise, and export point clouds, we chose to use the open-source

CloudCompare software (Girardeau-Montaut, 2015). The same tasks can also be accomplished by using proprietary software such as TerraSolid (Korzeniowska and Łącka, 2011).

Because the backpack LiDAR device we used has an effective scan range of around 200 m (over 180 million points were collected in a single field), the mapped area (over 1.5 ha, **Fig. 1d**) was much larger than the experiment region (i.e. the combined area of the 486 wheat plots, 0.5 ha). Hence, we used RTK-recorded geo-coordinates to delineate regions of interest (ROI) and facilitate our routine processing. After defining the ROI (over 45 million points retained for the experimental region, around 90,000 points per plot), all 3D points were visualised and coloured according to their z values (**Fig. 1e**). A preview of uncalibrated 3D mapping data prior to terrain adjustment enabled us to: (1) associate pseudo-colour to raw 3D points for quick growth assessment; (2) perform initial comparisons of experiments at multiple sites; and (3) define ROI to facilitate field- and plot-level 3D points sampling.

*A comprehensive pipeline for traits analysis*

To carry out routine 3D points processing and trait analysis using LiDAR-collected point clouds, we developed a comprehensive analysis pipeline. **Figure 2** shows a high-level workflow of the pipeline, which consisted of six steps: data selection, normalisation, the generation of crop canopy height model (CHM), plot segmentation, 3D trait analysis, and export of the analysis results:

1) *Step 1*: a pre-processed point cloud file (in LAS format) was selected (**Fig. 2a**). Because LiDAR-collected point clouds is likely to be noisy and uncalibrated (with slopes and terrain features of the field), we developed a process to normalise the 3D points (*Steps 2&3*). To remove noise, we followed a published method (Su et al., 2019), which calculates the average distance between a given 3D point and its neighbouring points (*avg.*). If the distance (*k*) between the point and its neighbouring points (defaulted to 50) is greater than $avg. + k \times std.$ (where *std.* is one standard deviation of the mean of all the distances), the point will be classified as an outlier. In our case, all identified outliers were coloured red and removed from the following analysis (**Fig. 2b**).

2) *Step 2*: after denoising, a filtering method was applied to separate ground-level and above-ground 3D points by applying the `LidarGroundPointFilter` function in WhiteboxTools (Lindsay, 2016), including (1) ground-based slope normalisation; (2) a subsequent k-nearest neighbours, kNN, (Lowe, 2004) to identify neighbouring points within a defined *radius* (defaulted to 2) to examine height differences; and (3) a classification method to classify ground-level and above-ground points. The use of the function resulted in a flattened ground plane, enabling precise measurements of above-ground 3D points. The output of *Step 2* is saved in a new LAS file with all the ground-level points assigned with *zero* z-values (dark blue) and above-ground points assigned with height values in centimetre (cm).

3) *Step 3*: a key step in the pipeline used to generate a CHM for 3D trait analysis. First, because the density of LiDAR-collected point clouds is likely to be unbalanced (e.g. denser 3D points for objects close to the laser scanner, **Fig. 1d**), we improved a progressive triangulated irregular network (TIN) algorithm (Zhao et al., 2016) to interpolate the unbalanced point clouds. Then, we utilised all the filtered above-ground points to generate a digital surface model (DSM), followed by the conversion of geo-coordinates on the x and y axes into pixel coordinates (Ritter and Ruth, 1997) to define four ROI markers in the DSM (**Fig. 2c**). When processing a series of point cloud files collected from the same field, these four markers could be used repeatedly. To reduce computational complexity, we associated z values of each 3D point with a grayscale value (i.e. 0 cm is taken to be black, and 160 cm is taken to be white; the taller the point, the higher the grayscale value), followed by a projection method to cast all 3D points onto the flattened ground plane. This process produced a 2D CHM image from an overhead perspective (**Fig. 2c**). Finally, we performed a 2D perspective transform (Mezirow, 1978) using the `getPerspectiveTransform` function in OpenCV (Howse, 2013) to extract the region within the four markers and then align the CHM for automated trait analysis. The 2D CHM image contains spatial information of all the plots in the experimental field.

4) *Step 4*: to segment plots using the 2D CHM, we employed the 2D Hough transform (Duda and Hart, 1972) to detect plot boundaries. Because the gap between plots could be unclear during the season (e.g. lodging could cover the gap), missing pixels between plots or noise could affect the result of the Hough transform. Hence, we designed an improved method to detect horizontal and vertical lines separately (**Fig. 2d**), including: (*Step 4.1*) combining both global (Sauvola and Pietikäinen, 2000) and local thresholding (Firdousi and Parveen, 2014) methods to establish an initial plot mask for the CHM, even if the background is not uniform; (*Step 4.2*) using the *Sobel* operator (Kroon, 2009) to detect the horizontal and vertical edges (angles were set at 360 and 30 as all the CHMs were aligned); (*Step 4.3*) drawing straight lines based on the detected edges (with right angles, x- and y-intercept as input parameters) using the `hough_line` and `line_aa` functions in Scikit-Image (van der Walt et al., 2014); (*Step 4.4*) merging multiple detected lines if they were close to each other, so that only a single line could represent the gap between plots (**Fig. 2e**). Finally, assembling the lines and producing a final plot-level mask to present all of the plots in the field (e.g. 162 plots in **Fig. 2e**). To remove edge effects, gaps within plots due to plant sampling, and crop variation that is not directly linked to the varieties or treatments (e.g. N loss), we calculated the weighted centroid of each plot using grayscale-based entropy features (Susan and Hanmandlu, 2013) within a given plot . Through this approach, width and length of a plot mask could be adjusted adaptively to rectify the plot-level sampling areas.

5) *Steps 5&6*: the last two steps of the pipeline measured and exported key performance- and yield-related traits for each plot. A range of traits have been measured, including crop height, 3D canopy uniformity, 3D canopy surface, canopy coverage and biomass estimation (i.e. 3DVI and 3DPI). A table (in CSV format) was generated and populated with these scores, with each row corresponding to a plot (i.e. a variety) and each column corresponding to a trait, arranged according to the plot location (i.e. row and column IDs) in the field (**Fig. 2f**).

*The GUI of CropQuant-3D*

To facilitate non-expert users to process 3D point clouds (in LAS format), we developed the GUI of CropQuant-3D, which integrated the above analysis pipeline into a single dialogue panel, from which all the above algorithmic steps could be performed. The GUI was implemented using PyQt5, a comprehensive set of Python bindings for the Qt v5 library (Summerfield, 2015), allowing the GUI to be executable on varied operating systems (see **Availability and requirements**). Following a similar systems design described previously (Zhou et al., 2017a), CropQuant-3D uses a stepwise approach to process point clouds and analyse 3D traits. The initial window (**Fig. 3a**) shows several sections with default input parameters pre-populated. In the input section, a user needs to select a LiDAR file (test LAS files provided on the GitHub). Then, the user needs to pre-process the selected point cloud file, including denoising and ground-based filtering (*Steps 1 & 2* in the GUI). After pre-processing, the user can generate a 2D CHM (*Step 3*) by defining the exchange rate between a pixel and a metric unit (i.e. cm), followed by defining geo-coordinates of the experimental field (i.e. ROI markers; *Step 4*). The *Step 5* is to segment plots using the 2D CHM, so that traits such as plot-based height and canopy coverage can be measured (*Step 6*). Finally, if the user needs to export point clouds for specific plots, the user can click four corners of one or multiple plots in the CHM following the order, upper-left, upper-right, lower-left and lower-right (*Step 7*, optional). To enable a fast selection of plot-level 3D points, we used the `EVENT_LBUTTONDOWN` function in OpenCV to create a mouse response event. The analysis results can be downloaded after all the mandatory steps are accomplished (**Fig. 3b**).

When a step is finished, a green-coloured message will be displayed in the section together with a Display button to show intermediate results (**Fig. 3c**). In particular, if the plot boundaries are unclear and the plot segmentation algorithm fails to segment all the plots, the user can define the field layout (i.e. the number of rows and columns) through an optional input box, which will generate base lines to assist the plot segmentation. Furthermore, to enable the GUI software to process point clouds produced from other sources such as UAV-SfM photogrammetry and LiDAR mounted on gantry systems, we expanded the input function to accept these types of point cloud files (in LAS format). For example, the CropQuant-3D GUI can process point clouds generated by both UAVs (**Fig. 3d**) and FieldScan™ (Phenospex, Netherlands; **Fig. 3e**) through unified analysis steps in the software to

perform plot-based 3D trait analysis. A detailed step-by-step user guide (**Supplemental Methods S1**) and an instructional video (**Supplemental Movie S1**) for the GUI-based software can be seen in the **Supplemental Data**. The software implementation can be seen in the **Materials and Methods** section.

*Height measurement using CropQuant-3D*

Plant height and the rate of height increase (i.e. growth rate) are important performance- and yield-related traits (Holman et al., 2016; Nguyen and Kant, 2018; Momen et al., 2019). For field-based phenotyping, we found that, although terrain adjustment (e.g. slope removing) is a standard process for height estimates from elevation models in large-scale land surveillance and forestry research, there are no standardised approaches designed for such adjustment in relatively small-scale crop fields. Hence, we have implemented a customised solution to normalise slopes and terrain features before height mapping. To measure crop height in a given plot, our algorithm was partially based on a mobile laser scanning approach described previously (Friedli et al., 2016), but performed on a flattened ground plane (*Steps 3&4* in the pipeline) with the highest 10% 3D points ($H_{10}$) sampled in the plot to reduce height variances at the canopy level. The average height value of the $H_{10}$ set was computed as the plot-level crop height. We produced three sets of height maps for all the six-metre 486 plots under three N treatments at the heading stage, with a unified height scale bar (**Fig. 4**). The 3D DSM and 2D CHM images (**Fig. 4a-c**, left) show the 3D reconstruction and height distribution of the three N blocks, from 60-degree and overhead perspectives; whereas the coloured height maps (**Fig. 4a-c**, right) demonstrate how height of wheat plants responded to different levels of N treatments (**Supplemental Table S1**).

*3D Canopy surface and canopy coverage measures*

The rates of carbon gain through photosynthesis and water loss through transpiration of the canopy can be affected by changes in canopy structure, which can be used to explain crop performance and plants' responses to environment (Green et al., 1985; Shearman et al., 2005). However, it is challenging to measure canopy structural characters due to its complexity and dynamic spatial

variability caused by genetic, agronomic management, and environmental effects (Omasa et al., 2007; Hosoi and Omasa, 2009; Duan et al., 2016). Although LiDAR devices have been used to visualise 3D canopy structure, how to quantify structural changes using point clouds was still a challenge that needed to be addressed.

We approached the matter through measuring a range of traits at the canopy level, including 3D canopy surface area and canopy coverage. To measure canopy coverage index, we developed the following steps: (1) retaining highest 50% 3D points ($H_{50}$) in a given plot (**Fig. 5a**); (2) then, projecting $H_{50}$ points onto a flattened plane to generate a 2D canopy image from an overhead perspective; (3) after that, applying the `threshold_local` function in Scikit-Image (Singh et al., 2012) to select pixels in the canopy image using the calculated local threshold, resulting in a binarized canopy mask to represent the canopy coverage in a plot. We applied the trait to measure the canopy coverage differences of a wheat variety (e.g. NMzi-1019) under three N treatments. The canopy coverage index (0-1, where 1 is 100% coverage) showed an increase of 10-15% when the N fertilisation increased (**Fig. 5b)**.

While the canopy coverage is important as it relates to the interception of direct solar radiation, it does not account for the total leaf area of the canopy, which is a more precise measure of interception of diffuse radiation and reflected light within the canopy (Cabrera-Bosquet et al., 2016). As the 3D surface area of the canopy would be closely related to the total transpirational leaf area and would correspond with the summed photosynthetic activity of all leaves (Omasa et al., 2007), we therefore included the measurement of 3D canopy surface area in the CropQuant-3D (**Fig. 5c**). The algorithmic steps were designed based on the triangle mesh method (Edelsbrunner et al., 1983), including: (1) applying the voxelization method (Truong-Hong et al., 2013) to generate a 3D grid system to package all the above-ground 3D points into voxels; (2) using the `voxel_down_sample` function from Open3D to down-sample the number of voxels, so that gaps between plants in a given plot could be covered; (3) using the `create_from_point_cloud_alpha_shape` function (Edelsbrunner et al., 1983) to reconstruct 3D surfaces of the canopy, followed by the `get_surface_area` function to calculate the 3D surface area. For example, the 3D surface area indices of wheat variety NMzi-1019

showed an increase of over 20% with the increase in N application levels (**Fig. 5d)**. In addition to the above two traits, we also integrated traits such as 3D voxel index (3DVI) and 3D profile index (3DPI) into CropQuant-3D to estimate biomass, which has been described previously (Jimenez-Berni et al., 2018; Deery et al., 2020). All the above trait analysis results are listed in **Supplemental Table S2**.

*An original canopy structural measure – 3D canopy index*

Whilst the above indices are useful measures to describe some canopy structural features, they do not convey information about canopy-level changes in spatial characteristics (e.g. height variation) across the plot, which are likely to be affected by many factors in the field experiments, including: (1) plant architecture such as individual tillers (e.g. main stem is taller than secondary tillers), which could differ between genotypes; (2) the height of spikes if a mixed population was drilled; (3) the density of the crop (e.g. spikes number per unit area, SN $m^{-2}$) due to different management practices such as the seeding rate, (4) agronomic or environmental reasons unrelated to treatment or genotype (e.g. local seedbed variations), and (5) lodging. We have established an original algorithm incorporated in the CropQuant-3D software to measure spatial differences at the canopy level. Following the previous naming convention (Jimenez-Berni et al., 2018), we called this measure 3D canopy index (3DCI). The algorithm for 3DCI consists of five key steps:

1) Using the plot-level masks (**Fig. 2e**), we extracted all the above-ground 3D points in a given plot to generate a pseudo-colour spatial map from an overhead view. We then transformed the map into a grayscale image with each pixel's grayscale value corresponding to its height value, resulting in a 2D plot-level CHM (**Fig. 6a**, right).

2) A 2D discrete Fourier Transform (DFT) method (Cooley and Tukey, 1965) was applied to represent the plot-level CHM in the frequency domain, producing the magnitude of the image's Fourier transform. Because the dynamic range of the Fourier coefficients was too large to be visualised, we applied a logarithmic transform and generated a frequency spectrogram (**Fig. 6b**),

containing all frequencies of the spatial information in the plot and their magnitude. The DFT can be defined as:

$$f(x,y) = \frac{1}{MN}\sum_{u=0}^{M-1}\sum_{v=0}^{N-1} F(u,v)e^{j2\pi(\frac{ux}{M}+\frac{vy}{N})};\ x = [0, M-1], y = [0, N-1] \quad (1)$$

Where *f(x, y)* represents the M×N spatial domain matrix, and *F(u, v)* represents the DFT of *f(x, y)*. The coordinate system of *F(u, v)* is in the frequency domain.

3) We centralised the frequency spectrogram to remove periodic interference signals, resulting in a centralised magnitude image to represent the spatial information. For example, by applying DFT to CHM images under three N treatments, we could identify different structural features at the canopy level (**Fig. 6c**): (a) the magnitude of the low-N magnitude image became rapidly smaller for higher grayscale values (e.g. canopy objects such as wheat spikes), suggesting its canopy was lower and the distribution of its spatial features was spread out (i.e. less dense) compared with crops under medium or high N treatments; (b) the main values of spectrogram images for both medium and high N applications lay on a vertical line, suggesting their canopy structures contained a dominating vertical orientation caused by regular patterns (e.g. lines formed by plants); and (c) in the medium-N magnitude image, another pattern could be observed which passed through the center at 75-80° angle (highlighted by a light-green dashed oval), which was caused by another spatial pattern in the plot and potentially could be a useful tool to measure the degree of lodging (**Fig. 6a**).

4) To utilise the above DFT results in quantitative trait measurements, we sampled all the pixels' grayscale values on the diagonal of the centralised magnitude image (red coloured lines in **Fig. 6c**), based on which frequencies of all spatial values and their amplitude were summarised. We then used the Gaussian fitting to plot the amplitude of the sampled spatial values, producing curves to represent canopy structural features within a defined frequency region, where the x-axis denotes frequencies of canopy-level spatial values, and the y-axis represents their associated amplitude (**Fig. 6d**). Two important features could be concluded from canopy structural curves:

(a) the curvature of these curves, signifying the density of crop canopy, as a less dense canopy structure contained larger spatial variation (e.g. less dense spikes) and resulted in a higher curvature ; (b) the area beneath the structural curve (e.g. with light red diagonal stripes, **Fig. 6d**), showing the canopy uniformity – when curvatures are similar, structural curves comprise greater area indicates less uniformity due to greater accumulated spatial variances. We used integral calculus (i.e. integration) to compute the area beneath the canopy structural curve, which is defined by Eq.2:

$$\int_a^b f(x)d(x) \approx \sum_{k=1}^{N} \frac{f(x_{k+1})+f(x_k)}{2} \Delta x_k;\ x \in [a,b], k = [1,N] \quad (2)$$

Where *x* is frequencies of spatial values, *a* is the minimum frequencies of spatial values (set as -100), $b$ is the maximum frequencies (set as 100), $f(x)$ is the amplitude value after Gaussian fitting, *N* is the total number of x sampled, $\Delta x_k$ is the difference between $x_k$ and $x_{k+1}$.

To compute the curvature of a structural curve, we used Eq. 3 as described previously (Van Der Walt et al., 2011):

$$Curvature = (|\frac{d^2x}{dt^2} * \frac{dy}{dt} - \frac{dx}{dt} * \frac{d^2y}{dt^2}|)/(\frac{dx}{dt} * \frac{dx}{dt} + \frac{dy}{dt} * \frac{dy}{dt})^{3/2} \quad (3)$$

Where *x* represents the frequency array (the x-axis), *y* is the amplitude array (the y-axis).

5) To use the above equations for measuring canopy uniformity, we normalised values generated by Eq2., so that we could cross-validate the measure for different varieties. We called this normalised value 3DCI. The normalisation is defined by Eq4.:

$$y = \frac{x - MinValue}{MaxValue - MinValue} \quad (4)$$

Where *x* is the calculated value using Eq2., *y* is the normalised 3D canopy uniformity index, *MinValue* is the theoretical minimum value from the value list, i.e. 59.3% of the calculated minimum value (Raybould and Quemada, 2010); and *MaxValue* is the theoretical maximum value from the value list, i.e. 129.4% of the calculated maximum value.

To verify the 3DCI and curvature measures, we used the wheat variety NMzi-1019, which has shown to respond strongly to different levels of N fertilisation (Feng et al., 2008). Three canopy structural curves of NMzi-1019 under three N treatments (n = 9 plots) were produced (**Fig. 6d**). The three curves' curvatures reduced moderately when the N fertilisation increased, indicating the canopy density were increasing. The high-N canopy curve (coloured red; 3DCI = 0.471) contained less accumulative spatial variation than those with low (coloured blue; 3DCI = 0.554) and medium-N (coloured light green; 3DCI = 0.513) treatments (see cross sections in **Fig. 6d**) and hence possessed a smaller area beneath the curve. Trends in 3DCI scores across N treatments could also be used to differentiate varietal differences in canopy responses to N treatments. For example, increasing 3DCI indicated that the canopy became more variable in height, suggesting more structural responses to N applications. Similarly, if the index decreased sharply with the N increase, this indicated that the crop canopy became more uniform rapidly and likely much denser when the N application changed.

*Validation of the CropQuant-measured traits using ground truth data*

Height estimates derived from the CropQuant-3D output were validated by comparisons with manual height measurements taken at the same stage of crop development (grain filling) in the 2019/20 trial. There was a strong correlation between the CropQuant-3D's height scores and manual measurements for each level of N, using plot-based (the square of the correlation coefficient, $R^2$, ranges from 0.69 and 0.87; *p*-value in linear regression analysis is less than 0.001; **Fig. 7a**; **Supplemental Table S3**) and variety-based means ($R^2$ ranges from 0.84 and 0.92, $p < 0.05$; **Fig. 7b**; **Supplemental Table S4**). Thus, the CropQuant-3D height scores based on the backpack LiDAR provides a viable alternative to manual height measurements, particularly for obtaining genotypic means. It is interesting that CropQuant-3D tended to underestimate the height for wheat varieties that are taller than 90 cm (some landraces were included). This is likely due to the way manual measurements were taken, which involved lifting and straightening curved or lodged plants to measure the distance from the soil surface to the tip of the ear along the vertical stem, whereas the LiDAR system measured the plants as they were naturally in the field. Furthermore, because only a limited number of plants were measured

in each plot manually, compared with a whole plot scan conducted with the backpack LiDAR, there is greater chance of plot-to-plot variability with the manual approach than with LiDAR, which integrates height measurements over a larger number of plants in a plot. Also, better variety-based correlation values might be due to height values for each variety have been averaged (three replicates per variety), reducing the height variance caused by treatments and small agronomic differences.

To verify the biological relevance of the 3D canopy surface area index, we have analysed correlations with plot-level grain number (GN $m^{-2}$) and grain yield (GW $m^{-2}$) using data collected from the 11 selected varieties (n = 81 plots). Strong positive correlations between this LiDAR-derived trait and the yield components, with $R^2$ ranging from 0.71 to 0.76 ($p < 0.001$, **Fig. 7c**; **Supplemental Table S5**), suggest a mechanistic link between the canopy trait and grain formation underlying the correlation, indicating that the 3D surface area index can serve as a good predictor of dynamic varietal performance. Additionally, there was a strong negative correlation between 3DCI (designed to quantify canopy uniformity and density) and manual measured spike density (SN $m^{-2}$) trait, with $R^2$ ranging from 0.77 to 0.81 ($p < 0.001$, **Fig. 7d**; **Supplemental Table S6**). Hence, it is likely that the 3DCI could also be used as a measure to quantify how SN $m^{-2}$, a key yield component, responds to different N applications, but without the slow and laborious process of manually counting spikes in the field.

*A case study of classifying nitrogen responses for wheat*

To effectively select crop varieties with an improved N response (e.g. high nitrogen use efficiency, NUE), it would be valuable to make use of proxy traits that are related to NUE under field conditions (Sylvester-Bradley and Kindred, 2009; Pask et al., 2012; Nguyen and Kant, 2018). The range of variables (e.g. 3D canopy surface area, canopy coverage, plot height and 3DCI) measured by CropQuant-3D were used jointly to describe canopy structural responses to three N treatments, which have enabled us to classify the N response of 11 selected wheat varieties (81 plots) into four classes (**Fig. 8**). The example varieties were as follows:

1) Class 1 – canopy structural curves differed across all three N levels. The patterns for ZM-4 could be clearly separated under the three N treatments (**Fig. 8a**), indicating that this type of wheat variety had a strong structural response to varied N applications at the canopy. Both 3DCI (coloured according to their associated N treatments) and the curvatures of the three canopy curves reduced steadily together with the increase of N, indicating that spike density and canopy uniformity were both rising in response to the escalation of N treatment. Also, the decrease of 3DCI corresponded with a continual increase of the SN $m^{-2}$ reading. Other lines from the 11 varieties that can be categorised into Class 1 are NMzi-1019, ZM-5 and ZM-11 (**Supplemental Figures S1**).

2) Class 2 – canopy structural curves were similar at low and medium N levels, but differed at high N. The patterns for NMzi-1 showed that the line had a good response to increased N, but only above the medium rate of N fertilisation. Both 3DCI and SN $m^{-2}$ suggested that low and medium N had similar effects on the variety (**Fig. 8b**). The SN $m^{-2}$ scores increased distinctly only under high N. Other lines that can be categorised into Class 2 are ZM-10 and ZM-12 (**Supplemental Figures S2**).

3) Class 3 – canopy structural curves were similar at medium and high N levels. The patterns for NM-8 suggested that the variety had similar responses under medium and high N treatments, indicating the increasing N fertilisation was not able to increase the line's spike density beyond the medium rate of N fertilisation (**Fig. 8c**). The other line that can also be categorised into Class 3 is ZM-26 (**Supplemental Figures S3**).

4) Class 4 – canopy structural curves decreased at high levels of N and showed the best response at medium N. Curvature patterns of ZM-168 indicated that the line had a similar canopy density at medium and high N treatments. The canopy uniformity was greater at the medium N level (3DCI = 0.506; **Fig. 8d**) and the line's spike density was the highest among the three N treatments. The other line that can be categorised into Class 4 is ZM-09196 (**Supplemental Figures S4**).

After classify N response patterns, we then combined 3DCI, crop height, canopy surface index area with the yield components, GN $m^{-2}$ and SN $m^{-2}$, to produce a performance matrix to understand crop responses to different N treatments in a compound manner. In the matrix, each variety was ranked based on the performance of these measures and traits. For example, by calculating the deviation of them based on the trimmed mean values (i.e. 15% over the trimmed mean coloured dark orange and placed in rank order 5, the highest rank; 7.5~15% coloured light orange and placed in rank 4; -7.5~7.5% coloured yellow and placed in rank 3; -15~-7.5% coloured light blue and placed in rank 2; and -15% below the trimmed mean coloured dark blue and placed in rank 1, the lowest rank), we could select lines with a desired performance under the three N treatments using a ranking system. In particular, for crop height, both very short and very tall were ranked undesirable (i.e. placed in rank 1), whereas both GN $m^{-2}$ and SN $m^{-2}$ were given more weight (Langer and Liew, 1973) than other measures ($weights = [0.25, 0.25, 0.2, 0.1, 0.2]$). Through the ranking system, we concluded that: (1) for the low N treatment, ZM-168 achieved a more balanced score in terms of grain production and structural variation (**Fig. 9a**); for the medium N application, NM-26 ranked the highest (**Fig. 9b**); and, for the high N, NM-26 was scored the highest (**Fig. 9c**). Although this is only an initial attempt for selecting wheat varieties with desirable N responses using LiDAR-derived traits and key yield components, it is evident that the performance matrix could provide an objective approach to rank multiple wheat varieties. Further validation and field studies using the above approach are ongoing and will be reported separately.

**Discussion**

Plant phenomics is an important area that helps provide valuable phenotypic information that is needed to fully exploit available genomic resources. For crop improvement programmes, the focus is on multi-location and large-scale field phenotyping, yet there are a number of weaknesses with current solutions (Tardieu et al., 2017; Furbank et al., 2019; Pieruschka and Schurr, 2019), concerning: (1) mobility (a method can be straightforwardly used in multiple locations); (2) affordability (whether

purchase, operation and maintenance of a system can be afforded by research groups with acceptable resources); (3) throughput (the number of plots, traits and fields that can be measured within a reasonable time frame, as well as the number of times to phenotype in a growing season); (4) accuracy (the information truly relates to the target attributes or biological functions of the plant); (5) resolution (if the method provides information at the level of detail required to test the biological hypothesis); and (6) scalability (the size of trials that can be phenotyped and the number of locations that can be covered).

In addition to data collection, another issue that limits the use of field phenotyping tools involve the ability to analyse big data acquired from the field (Kelly et al., 2016; Scharr et al., 2016; Cendrero-Mateo et al., 2017; Lobet, 2017). Although many open-source and proprietary software solutions have been developed (Butler et al., 2020; Roussel et al., 2020), their applications are normally limited to certain devices and for specific research questions, leading to matters such as software usability, data interoperability, and the generalisability (Carpenter et al., 2012; Roitsch et al., 2019). To address some of the above issues, we pioneered the integration of backpack LiDAR and an open-source software implementation to measure genotypic and N treatment differences in spatial features in wheat. Results from field experiments showed that structural measures (e.g. height, 3DCI, and canopy surface area) are highly correlated with key yield components such as SN $m^{-2}$ and GN $m^{-2}$, indicating the system could be used as a reliable research tool to classify the plant responses to different N treatments.

*The backpack LiDAR hardware*

We have shown that the backpack LiDAR device introduced here is integrated and portable, enabling the collection of high-density 3D point clouds at the field and plot levels. Typically, these kinds of data would require LiDAR systems to be mounted on a gantry or vehicle platform, which are often not available, too costly, fixed in one location, or cannot reach fields with limited accessibility. To our knowledge, the backpack LiDAR system has not been used in field-based plant phenotyping previously. Hence, we developed a range of techniques to apply the device in wheat field experiments. Our field testing and development experience show that the backpack LiDAR possesses three notable

599 features: (1) large-scale capability (up to 210 m effective scan range through our equipment), with an
600 acceptable mapping speed (up to 1.2 ha per hour); (2) portability (the ability to conduct multi-location
601 phenotyping) with limited adjustments of hardware and software; (3) relatively small operation and
602 maintenance costs due to its integration, ease-of-use and mobile features. Hence, backpack LiDAR
603 appears to provide a more balanced solution to some current phenotyping challenges. Although
604 backpack LiDAR, like most high-resolution LiDAR systems with high-end scanners, is still relatively
605 expensive. However, costs should decrease and become more affordable as the technology matures
606 (Su et al., 2020). Comparisons between backpack LiDAR devices and other approaches can be seen in
607 the section below.
608
609 *CropQuant-3D software and trait analysis*
610 Processing of 3D point cloud data collected by LiDAR systems for 3D trait analysis is still
611 complicated and computationally demanding, indicating the necessity of reliable analytic solutions.
612 Furthermore, for solutions that can be used by non-experts and widely accessible by the plant research
613 community, the software should be user-friendly and openly available. Therefore, we developed the
614 CropQuant-3D analysis software to routinely process large point cloud datasets. To help other
615 researchers exploit our analysis algorithms integrated in the software, besides the GUI software, we
616 also modularised the analysis tasks into individual procedures and then saved them with executable
617 Python source code in Jupyter notebooks that can be executed on multiple operating systems. The
618 algorithmic steps include pre-processing of 3D point clouds (**Supplemental Methods S2**), automated
619 plot segmentation with optional experimental layout input, and plot-level crop height (see
620 **Supplemental Methods S3**), 3D trait analysis of canopy structural features (3DCI, 2D canopy
621 coverage, 3D canopy surface area), and biomass estimation such as 3DVI and 3DPI (see
622 **Supplemental Methods S4**). Compared with previously work (Ward et al., 2019; Hyyppä et al., 2020;
623 Su et al., 2020), we have made progress in several areas for large-scale 3D trait analysis in plants:
624
625 1) Due to the huge volume of raw point cloud data collected, efficient data processing needs to be
626 considered for both throughput and accuracy. Many existing methods require much computational

time to pre-process point clouds. In our case, we have chosen to use a ground-level filter with parameters tailored for small-scale crop field, retaining only 3D points required by trait analysis. This approach noticeably reduced processing time. For example, for a 400 MB LiDAR file (over 15 million 3D points), only 100-120 seconds were required to normalise 3D points on an ordinary computer (intel i7 CPU and 16 MB memory; see profiling in the **Material and Methods**).

2) We analysed plot-level 3D traits using 2D CHM, which retains sufficient spatial information in 2D pixels. This approach enabled us to employ computationally more efficient 2D-based algorithms such as edge detection, Hough transform, and adaptive thresholding to perform plot segmentation and trait analysis, reducing the computational complexity. Another key benefit for this 3D-to-2D transformation is that analysis regions could be controlled dynamically in any plot region. By calculating the texture entropy (Haralick et al., 1973), we could compute the weighted centroid of a plot and then define the sampling area according to experimental needs.

3) Since the density of the LiDAR-collected 3D points is likely to be imbalanced (e.g. the further away from the mapping route, the sparser the 3D points), it is necessary to interpolate the point clouds if the number of 3D points in a given plot is limited. From a range of interpolation algorithms, we have chosen the progressive TIN to build a TIN-based model and then densify 3D points in an iterative manner, which helped us improve the quality of 3D trait analysis while retaining key 3D geometric features at the plot level.

4) It is technically difficult to describe 3D canopy structure in a quantitative manner. The 2D Fourier transform method employed by CropQuant-3D opens a door to quantify spatial variances, spike density and uniformity at the canopy level by dividing frequency and amplitude of all height values across the plot. A similar idea but with a different approach can be found in measuring the canopy roughness of leafy trees in forest ecology (Antonarakis et al., 2010). Our approach was able to show that, through the canopy structural curve and 3DCI (**Fig. 6d**), we could quantify the uniformity and density of wheat spikes in plots, which could be used to classify varieties

according to different responses to N treatments and potentially other treatments. Meanwhile, the curvature of the canopy curves can also be employed to help distinguish the canopy density in relation to different N treatments and varieties.

There are many vision-based approaches developed to mine spatial and temporal features from point clouds for a range of biological questions, for example, identifying phenotypic differences at the organ level (Li et al., 2020a) and the extraction of single plants within a plot (Jin et al., 2021). Because our research aim was to enable large-scale field phenotyping for plot-level 3D trait analysis, we therefore did not consider plant-level 3D reconstruction and methods to analyse detailed features (e.g. plant-level marching cubes, leaf curvature estimation, and 3D skeletonization) in this work.

*Wheat varietal responses to different nitrogen fertilisation levels*

NUE in crops is generally low. Approximately 40% of the applied N can be utilised by cereal crops, with the bulk of the remainder leaching to groundwater or volatilising to the atmosphere, causing increased agricultural costs and negative impacts on the environment (Raun and Johnson, 1999; Good et al., 2004). Breeding crop varieties with improved NUE should contribute to more sustainable cropping systems. To effectively select lines with heritable NUE-related proxy traits under different field conditions, it is technically difficult to screen many complex traits due to their dynamics and complexity (Good et al., 2004; Sylvester-Bradley and Kindred, 2009).

In the case study, we have explored a comprehensive procedure to quantify N responses of different wheat varieties based on phenotypic traits and key yield components. When the level of N changed, different varieties varied with their responses in terms of canopy structural features and key yield components. By combining key yield components and LiDAR-derived trait values, we identified four NUE types using the subset of 11 varieties: (1) grain yield responded well to increased N applications (Class 1); (2) only higher N was able to increase yield (Class 2); (3) medium and high N treatments led to similar grain production (Class 3); and (4) higher N led to a yield decrease (Class 4). We believe that the combined performance matrix demonstrated in the case study is likely to help

682 establish an objective approach to identify wheat lines with superior N responses, which may lead to
683 an effective selection improvement of NUE in wheat breeding programmes in the future. Further work
684 to link this selection approach with yield production and NUE at a large scale is ongoing.
685
686 *Applications of CropQuant-3D*
687 The traits and measures here (e.g. height, coverage, canopy area, and 3DCI) do not just relate to N
688 treatments, but they also closely connect with many aspects of genetic variation in crop performance.
689 For example, crop height is an important factor in assessing risk to crop lodging, 3D canopy area and
690 2D ground coverage are good indicators for managing agricultural inputs to optimise canopy structure
691 for radiation capture, photosynthetic output and transpirational water loss. It is also important to note
692 that such traits are only apparent in the context of a population in plots, and most of these traits are
693 difficult or impossible to convey by phenotyping individual plants in controlled environments.
694 Canopy-level traits are affected by variety, soil characteristics and agronomic factors such as seed
695 spacing and the application of plant growth regulators. The accuracy of plant models that attempt to
696 simulate the effects of these factors and their interactions on crop performance could be improved by
697 supplying them with traits presented here that were collected across a wide range of scenarios.
698 The 3D traits derived from LiDAR data such as 3DCI have many underlying component traits and
699 spatial features. A better understanding of the bases of 3DCI would broaden its application for other
700 crop improvement programmes. For instance, height variances within a plot could be due to a variety
701 of reasons: 1) a mixed population of plants with different genes controlling height, or that major
702 height genes are not fixed, but still segregating in the population; 2) agronomic or environmental
703 variability within the plot that is not related to genotypes; and 3) as 3DCI is affected by height as well
704 as spike density, it is likely that the analysis of 3D point clouds could pick up the differences in height
705 of the mainstem, different tillers on each plant, and tillering responds both to N treatment and
706 genotype (Power and Alessi, 1978).
707 Another biological application of the CropQuant-3D system is for discovery of robust quantitative
708 trait loci (QTL) for agronomic traits, which requires phenotypic data on large mapping populations
709 across multiple field environments (Griffiths et al., 2012). The high-throughput capabilities of this

combined system are well suited to this scale of research. A similar research approach has been reported in our recent work, SeedGerm (Colmer et al., 2020), which was applied to detect genetic differences in *Brassica napus* based on a range of seed germination traits. Although more work is needed, greater automation of phenotypic analysis and improvements in accuracy are likely to accelerate genetic analysis of crop performance under varied treatments or environments.

Beyond existing 3D trait analysis, continuous phenotypic analysis in 3D of different crop species is likely to extend our understandings of the physiological bases of crop growth and development, for which the open-source nature of CropQuant-3D is likely to be valuable for the research community. There is an additional analytic power in examining longitudinal traits (time-series measures of traits that change as the crop develops and matures), which can describe the dynamic interactions between crop genotypes and N responses. By streamlining both the data acquisition and data analysis of field phenotyping with the backpack LiDAR and CropQuant-3D, it becomes possible to obtain measures at each key growth stage and at different test locations and environments, which was difficult to achieve with systems that are less portable and flexible in operation, with limited opportunity to expand or alter the use of the analysis software. With the approach introduced here, multi-environment 3D traits collected along a time series on large genotype collections could enable a deeper understanding of the genetic and physiological bases of efficient use of N for crop growth and development, as well as how these responses are modulated by the environment. Technically, other than some supervised machine learning algorithms, we have not embedded popular deep learning techniques into the analysis pipeline for 3D traits analysis. Continuous development will improve our work, opening 3D phenotypic analysis to non-expert users and computational biologists who are willing to extend and jointly develop the platform. Overall, we believe that the combined backpack LiDAR and CropQuant-3D system could have a great potential to advance large-scale and multi-location field phenotyping, 3D phenotypic analysis, and genetic studies for both crop research and breeding applications.

*Issues associated with the backpack LiDAR and CropQuant-3D*

Despite clear advantages, it is important to point out limitations of the combined solution. LiDAR technology has been maturing very rapidly in recent years. The Robin backpack LiDAR used in this

738 study is already being replaced by newer models with better accuracy, effective scan range, and a
739 lower purchase price (the price of LiDAR devices has decreased over 30% since 2018;
740 www.yole.fr/LiDAR_Market_Update_Livox_LiDAR.aspx). Although this type of LiDAR is more
741 affordable than other large-scale systems, it is worth noting that, depending on the laser scanner
742 integrated in a backpack LiDAR device, the equipment is still relatively expensive. We compared the
743 costs of Robin with some representative backpack LiDAR systems, as well as other LiDAR-based
744 mapping approaches (**Supplemental Table S7**; information regarding GPS and RTK accuracy can be
745 found via the links in the References column). However, it is also notable that the integration and
746 mobility features of backpack LiDAR possess a unique opportunity for the community to explore
747 shared services or community-driven facilitates encouraged by EMPHASIS and AnaEE (Roy et al.,
748 2017).

749 Additionally, our software was not designed to address many colour- or spectral-related traits that
750 are also important for crop performance. For example, senescence of the lower canopy due to
751 differential N or water limitation. Adjustments to how the LiDAR is used and the associated analysis
752 algorithms would be required to capture such traits in future work. However, similar issues can be
753 applied to most of the LiDAR systems. Moreover, it was difficult to scan the lower part of the crop
754 after the canopy closure, which could cause errors to estimate above-ground biomass with stems
755 included. Also, due to field conditions such as wind movement of the plants, it is extremely
756 challenging to generate a very high-resolution and high-precision 3D model to analyse an individual
757 plant within the plot, even with high-end laser scanners or close-up 3D mapping modes. Alternative
758 3D points registration algorithms are therefore needed to deal with plant movement and reliable plant-
759 level 3D modelling.

760 The CropQuant-3D system is capable of automating the segmentation of hundreds of plots for trait
761 analysis, but the algorithm is likely to fail at the seedling development and tillering stages (GS10~29).
762 This is because the early crop height map and the gaps between drilled plants are too big to ensure a
763 meaningful plot segmentation. However, as stems elongate and crop height increases (e.g. from the
764 jointing stage onwards, GS31), our system can perform reliable plot-level masking. Another technical
765 issue that needs to be taken into consideration is the request for a user to select plot(s) to extract plot-

level point clouds. Although plot-level point clouds are not required for the trait analysis reported here, a user is required to select one or multiple plots on the 2D CHM to extract associated point clouds, which can be laborious if point clouds from hundreds of plots need to be extracted. For this technical constraint, automated plot-level 3D points extraction is required and recent reports suggest they are within reach (Walter et al., 2019; Roussel et al., 2020; Jin et al., 2021).

Lastly, because we have applied the 3D-to-2D analysis approach, some spatial information might be lost during the 3D-to-2D transformation, which could reduce the accuracy when the research interest is beneath the canopy region. For this loss of accuracy during the transformation, we have performed some testing using 3D point cloud files collected by other equipment such as drone and vehicle mounted LiDAR (**Figs. 3d&e**) to carry out multi-scale point cloud processing. Although the preliminary is promising, further development and testing are still required to make the platform more compatible with these types of point cloud data. Next steps of the research also need to expand the application of CropQuant-3D to the analysis of different crop species so that the algorithms developed for wheat can be used for addressing similar biological problems in other crop species.

*Conclusion*

The requirement of obtaining accurate and meaningful measures of the field phenotype at sufficient scale, throughput, cost and multiple locations create a bottleneck in today's crop research and breeding, which is preventing us from making full use of genomic resources for crop improvement programmes. Backpack LiDAR has obvious advantages for large-scale field experiments and breeding trials. The device is easy to transport and use, overcoming the main limitations of fixed phenotyping platforms and can be used for multi-site data collection and at multiple time points. However, the ability to process and analyse large datasets with minimal time and standard computing power has limited the wide application of LiDAR-based phenotyping. To address this, we have developed CropQuant-3D, which processes large LiDAR-derived 3D point cloud data and consists of original algorithms packaged into a user-friendly GUI software to output multiple 3D canopy traits (e.g. 3DCI) at the plot level. In a case study of 11 wheat varieties grown under three levels of N inputs, analysis results obtained by by combining a backpack LiDAR and the CropQuant-3D software

showed that wheat varieties could be classified into different N response groups according to a range of 3D traits that relate to spike density (SN $m^{-2}$) and grain yield. This indicates that the combined solution could be a useful tool to make selections for NUE, and to dissect the physiological mechanisms and genetic regulation of NUE. Hence, we trust that the system presented here has a great potential to relieve some of the current bottleneck in large-scale field phenotyping for crop research and breeding.

## Materials and Methods

*Plant material and field experiments*

In the first season (2018/2019), 105 Chinese winter wheat (*Triticum aestivum*) varieties were planted at the Zhenjiang Agricultural Technology Innovation Center (ZATIC, 31°57'N, 119°18'E, Jiangsu province, China), measured using CropQuant-3D and assessed for yield and N responses. A subset of 54 varieties (**Supplemental Materials S9**) were chosen out of the 105 lines for the 2019/2020 season. The selected 54 Chinese winter wheat varieties used in the field experiments were cultivated from the wheat plantation regions of the middle and lower reaches of the Yangtze river, which were shown previously to vary in performance and yield under different nitrogen (N) treatments (Feng et al., 2008). A split-plot design was used, with three levels of N fertilisation as main plots, containing three replicates of the 54 varieties as sub-plots (162 plots per N experiment). The overall size of the 2019/20 field trial was 486 plots, covering approximately 0.5 ha (**Fig. 1a**). For the purposes of explaining the methods, data from 11 of the 54 varieties are shown.

*Crop management*

Before sowing, soil samples (for 0-25 cm soil layer) were measured to ensure that available N content was suitable for N response studies (**Table 2**). Following standard crop management guidelines (Godwin et al., 2003) and local practice, base fertiliser ($P_2O_5$ and $K_2O$) was applied before drilling. Three levels of N fertiliser treatments were applied by hand (0, 180, and 270 kg N $ha^{-1}$) in two splits: 50% at sowing and 50% at jointing (GS31). Crops were planted in 6 $m^2$ plots (2×3 m), with 6 rows per plot at 15 cm spacing, with 30 cm gaps between plots (**Fig. 1a**; trial plans in **Supplemental Table**

822 **S8**). The planting density was 2.4 million plants per hectare. Plant growth regulator was not applied in
823 the season so that stem elongation could respond unimpeded to different levels of N treatments.
824
825 *Manual measurement*
826 To collect reliable ground truth data for validating and improving CropQuant-3D's analysis algorithm,
827 a team of five field workers performed the manual scoring. They conducted a range of manual
828 measures at key growth stages (from heading, GS51-59, to grain filling, GS71-89), including plant
829 height, growth stage scoring, and key yield components such as spike number density (SN $m^{-2}$), spikes
830 per plant, grain number per unit area (GN $m^{-2}$), and thousand grain weight (TGW). For example,
831 manual plant height measures of five typical plants per plot were conducted on 11$^{th}$, 18$^{th}$ and 26$^{th}$ May
832 2020, from which the scores on 18$^{th}$ May (two days after the LiDAR mapping, 16$^{th}$ May 2020) were
833 used for correlation studies in this work. As there were variances in height across the plot, three one
834 metre-square regions were selected to represent height variances within a plot. Then, all plants in the
835 region were measured and the average height value was recorded as the plot height value. When
836 measuring the plant height, the distance from the ground to the top of the ear was measured with a
837 steel ruler. We took steps to standardise manual measurements: (1) cross-scoring same traits with
838 different field workers, (2) cross-validating scores across experiments using historic data, and (3)
839 using trimmed mean to remove outlier values before calculating the average of ground truth. At
840 maturity, yield was measured in a 1 $m^2$ quadrat centred in the plot, from which ears were removed
841 with a sickle. Threshing was carried out with a plot thresher; any grain that passed through the
842 thresher were manually recovered from the sieved straw.
843
844 *The backpack LiDAR system*
845 The backpack LiDAR (Robin Precision, 3DLasermapping; purchased by GeoSLAM, Nottingham, UK)
846 integrates a laser scanner (RIEGL VUX-1) and three mapping settings, employing accurate GPS-
847 tagged navigation, and was used in conjunction with a real-time kinematic (RTK) base station for
848 precise positioning. The system is a lightweight (around 10 kg) and comprises high-performance laser
849 mapping system (360$^o$ scanning angle with an effective scan range of 3-200 m; further detail

in **Supplemental Methods S5**). Measurements focussed on the key growth stages (Zadocks et al., 1974), from heading (GS51-59) to grain filling (GS71-89) when canopy structural features were largely established. Standard pre-processing software packages were bundled with the device. To capture the peak height for the selected wheat varieties, the trial was mapped from April to May 2020. In our preliminary work, similar 3D field mapping was conducted in paddy rice trials at the Tuqiao crop breeding and cultivation centre (Jiangsu China) and at the Chinese Academy of Sciences' (CAS) Songjiang crop research center (Shanghai China, **Supplemental Figures S5&S6**). CropQuant-3D is not bundled with Robin and can be used to analyse point cloud files generated by other sources.

*GUI-based software development*

To develop the GUI-based analysis software for CropQuant-3D, we utilised PyQt5, a comprehensive set of Python bindings for the Qt v5 library (pypi.org/project/PyQt5/), which was developed using C++ and is cross-platform for modern desktop (e.g. Windows and Mac OS) and mobile (e.g. Android and iOS) systems. The GUI software we developed follows a traditional desktop-based user interface development, which can be easily modified to operate in a web browser such as Google Chrome. Anaconda Python release (docs.continuum.io/anaconda/install/windows) was employed as our integrated development environment, through which third-party libraries required for the software implementation, testing and packaging were managed by multiple virtual environments installed into the `conda` directory (Virtanen et al., 2020). Algorithms (in Jupyter notebooks), GUI software (in EXE format), Python-based source code and testing files (in LAS format) are freely available.

*Software implementation*

To implement *Step 1* (denoising) in the analysis pipeline introduced in the **Results** section, we first used the `file.File` function in the laspy library to read the input file, followed by the `spatial.cKDTree` function in the Scipy library to index the 3D coordinates of all the points in the LAS file. Then, we applied the filtering criteria (i.e. $avg. + k \times std.$) to index outliers in the point clouds and saved the denoised point cloud data using the function `file.File` (in LAS format).

For the *Step 2* (filtering) in the pipeline, we developed three approaches to process point cloud files generated through different approaches: (1) for the backpack LiDAR mapping, we used the function **`lidar_ground_point_filter`** in the WhiteboxTools library to filter the point cloud; (2) for UAV-SfM generated pint cloud files, we employed the function **`do_filtering`** in the CSF library to separate ground-level 3D points from above-ground points; (3) for the gantry-mounted LiDAR files, because the 3D points have already been filtered, we could use the files directly.

For the *Step 3* (the generation of CHM) in the pipeline, we also developed three approaches to process different types of point cloud files: (1) for the backpack LiDAR generated files, we applied the function **`lidar_tin_gridding`** in the WhiteboxTools library to output CHMs with the resolution parameter set as 1 cm/pixel; (2) for UAV-SfM files, we used the **`lidar_tin_gridding`** function to output digital earth model (DEM) and DSM, followed by the **`clip_raster_to_polygon`** function to rectify the DSM and DEM's resolution using the shapefile (the .shp file collected by RTK), resulting in an CHM imaging produced through subtracting the DEM from the DSM; (3) for the gantry LiDAR files, the **`lidar_nearest_neighbour_gridding`** function was used to produce the CHM image.

For the *Step 4* (the definition of ROI) in the pipeline, we used the function **`read_csv`** in the pandas library to read the geo-coordinates of the point cloud files, followed by the **`open`** function in the rasterio library to open the CHM and convert the geo-coordinates to pixel coordinates so that 3D point clouds could be analysed in 2D. The function **`getPerspectiveTransform`** in the OpenCV library was employed to obtain the perspective transformation matrix together with the **`warpPerspective`** function in OpenCV to define the ROI in the 2D CHM. Finally, the **`io.imsave`** in the scikit-image library was used to save the aligned 2D CHM within ROI.

For the *Step 5* (plot segmentation) in the pipeline, the optional input parameters such as the number of rows and columns could be used to generate horizontal and vertical base lines to assist the plot segmentation. Using the **`threshold_sauvola`** and **`threshold_local`** functions in scikit-image, we could obtain the threshold mask of the CHM image. Then, we applied the **`sobel`** function in scikit-image to detect edges in the CHM, followed by the **`hough_line`** function to fit vertical and

horizontal lines, separately. By merging the detected lines and base lines, we could generate the final mask representing the plot boundaries in the field.

For plot-based 2D/3D trait analysis, we mainly used the `regionprops` function in scikit-image to calculate phenotypic traits in each plot. The plot-level 3D canopy traits were based on the `clip_lidar_to_polygon` function in WhiteboxTools to crop plot-level point clouds. The source code produced from the above software implementation can be seen in **Supplemental Methods S2-S4**, as well as from our GitHub repository.

*Software profiling*

We profiled the GUI software using a range of testing point cloud files (in LAS format, available on our GitHub repository), which were acquired by the backpack LiDAR (403 MB; 15,090,552 points), UAV SfM generated point clouds (596 MB; 18,372,420 points), and gantry LiDAR (FieldScan™, 1.42 GB; 58,446,207 points). Three Windows laptop computers with different hardware configurations were used for the software profiling: (1) Intel Core i5 with 8GB memory (budget laptop); (2) Intel Core i7 processor and 24GB memory (middle-end laptop); and (3) Intel Core i9 with 32 GB memory (high-end laptop). As the CropQuant-3D software did not support GPU acceleration, both CPU and memory influenced the processing performance of CropQuant-3D. By averaging the computational time (using the `time` module in Python) used by the three computers, we provided details on the processing time using the three types of testing files at each step (**Supplemental Table S10**).

**Availability and requirements**

Project name: 3D field phenotyping for wheat using backpack LiDAR and CropQuant-3D

Project home page: https://github.com/The-Zhou-Lab/LiDAR

Source code: https://github.com/The-Zhou-Lab/LiDAR/releases/tag/V2.0

GUI software: https://github.com/The-Zhou-Lab/LiDAR/releases/tag/V2.0

Programming language: Python 3.7

Requirements: Laspy (1.7.0), Whitebox (1.3.0), GDAL (3.1.4), Rasterio (1.1.8), Open3D (0.11.2), Mayavi (4.7.2), Scikit-Image (0.17.2), OpenCV-Python (4.4.0.46), Pandas (1.1.5), Numpy(1.19.4), Matplotlib(3.3.3), and Scipy (1.5.3).

License: The MIT License for open-source initiative (https://opensource.org/licenses/MIT)

**Abbreviations**

Comma-separated values (CSV), nitrogen use efficiency (NUE), internet of things (IoT), unmanned aerial vehicle (UAV), Light Detection and Ranging (LiDAR), three-dimensional (3D), computed tomography (CT), red-green-blue (RGB), global navigation satellite system (GNSS), canopy height model (CHM), Zhenmai (ZM), Ningmai (NM), operating system (OS), nitrogen (N), spikes number per unit area (SN $m^{-2}$), grain number per unit area (GN $m^{-2}$), thousand grain weight (TGW), real-time kinematic (RTK), global positioning system (GPS), regions of interest (ROI), k-nearest neighbours (kNN), graphical user interface (GUI), root-mean-square error (RMSE), discrete Fourier transform (DFT), Structure from Motion (SfM), 3D voxel index (3DVI), 3D profile index (3DPI), 3D canopy index (3DCI), research and development (R&D).

**Availability of supporting data**

The datasets supporting the results presented here are available at https://github.com/The-Zhou-Lab/LiDAR/releases/tag/V2.0. Source code and other supporting data are openly available on request.

**Supplemental Data**

**Supplemental Figure S1.** Canopy structural curves of four wheat varieties (n = 31 plots), ZM-4, NMzi-1019, ZM-5 and ZM-11, which were classified into Class One due to their similar nitrogen-response patterns.

**Supplemental Figure S2.** Canopy structural curves of three wheat varieties (n = 23 plots), NMzi-1, ZM-10 and ZM-12, which were classified into Class Two due to similar nitrogen-response patterns.

**Supplemental Figure S3.** Canopy structural curves of two wheat varieties (n = 15 plots), NM-26 and ZM-8, which were classified into Class Three due to similar nitrogen-response patterns.

**Supplemental Figure S4.** Canopy structural curves of two wheat varieties (n = 12 plots), ZM-168 and ZM-09196, which were classified into Class Four due to similar nitrogen-response patterns.

**Supplemental Figure S5**. The backpack LiDAR used in three experimental fields at Tuqiao field center (Jiangsu China), examining 1,458 1 $m^2$ rice plots under two levels of nitrogen treatments (i.e. 180 and 270 kg N $ha^{-1}$).

**Supplemental Figure S6.** The backpack LiDAR used in an experimental field at Songjiang crop research center (Shanghai China), examining 261 1 $m^2$ rice landraces.

**Supplemental Table S1.** CropQuant-3D-measured crop height values for 486 six-metre plots (54 wheat varieties with three replicates) under three nitrogen (N) treatments (0, 180 and 270 kg N $ha^{-1}$).

**Supplemental Table S2.** CropQuant-3D's traits analyses of 81 six-metre plots of ZM & NM varieties under three nitrogen (N) treatments (0, 180 and 270 kg N $ha^{-1}$), generated by the graphical user interface (GUI) based software.

**Supplemental Table S3.** Plot-based correlation performance metrics evaluate CropQuant-3D-measured height values using manual height measurement under three nitrogen (N) treatments (0, 180 and 270 kg N $ha^{-1}$).

983 **Supplemental Table S4.** Variety-based correlation performance metrics evaluate CropQuant-3D-
984 measured height values using manual height measurement under three nitrogen (N) treatments.
985
986 **Supplemental Table S5.** Correlation performance metrics evaluate CropQuant-3D-measured canopy
987 surface area trait using manual grain number per unit area (GN $m^{-2}$) scores under three nitrogen (N)
988 treatments.
989
990 **Supplemental Table S6.** Correlation performance metrics evaluate CropQuant-3D-measured 3D
991 canopy index (3DCI) trait using manual spike number per unit area (SN $m^{-2}$) scores under three
992 nitrogen (N) treatments.
993
994 **Supplemental Table S7.** Cost comparison between backpack LiDAR devices, unmanned aerial
995 vehicle (UAV) airborne LiDAR, and the handheld laser scanning system, with brief technical
996 specifications.
997
998 **Supplemental Table S8.** Three split fields used to study three replicates of 54 wheat varieties under
999 three levels of nitrogen (N) fertiliser treatments (i.e. 0, 180, and 270 kg N $ha^{-1}$). Crops were planted in
1000 six $m^2$ (2×3 m) plots, 486 plots in total.
1001
1002 **Supplemental Table S9.** Soil nutrient (0-25 cm soil layer) content measured before drilling in the
1003 2019/2020 season.
1004
1005 **Supplemental Table S10.** Processing time for three types of point cloud files, collected by backpack
1006 LiDAR, unmanned aerial vehicle (UAV) Structure from Motion (SfM) photogrammetry, and gantry-
1007 based LiDAR, at each analysis step.
1008

**Supplemental Methods S1.** A step-by-step user guide of how to use the graphical user interface (GUI) based CropQuant-3D software to perform 3D trait analysis of point cloud datasets collected by backpack LiDAR, unmanned aerial vehicle (UAV) Structure from Motion (SfM) photogrammetry and gantry-based LiDAR.

**Supplemental Methods S2.** Python-based code fragments for pre-processing LiDAR-collected point cloud datasets.

**Supplemental Methods S3.** Python-based code fragments for automatically segmenting plots using the pre-processed LiDAR point cloud datasets.

**Supplemental Methods S4.** Python-based code fragments for performing plot-based 3D trait analysis, including the measurement of canopy structural variation such as 3D canopy index (3DCI).

**Supplemental Methods S5.** The introduction of the backpack LiDAR device, Robin Precision™, used in this study.

**Supplemental Movie S1.** An instructional video showing how to use CropQuant-3D in action.

**Acknowledgements**

The authors would like to thank all members of the Zhou laboratory at the Nanjing Agricultural University (NAU, China) and the Cambridge Crop Research, National Institute of Agricultural Botany (NIAB, UK) for fruitful discussions and cross-disciplinary collaborations. In particular, the authors would like to thank Prof Roger Sylvester-Bradley at ADAS, Dr Stéphanie Swarbreck at NIAB, and Prof Simon Griffiths at the John Innes Centre (JIC) for proofreading and helping us improve the manuscript. We also thank Prof Han Bin at the Chinese Academy of Sciences, Prof Dong Jiang, Prof Xiu-e Wang, Prof Daolong Dou, and Prof Yuqiang Liu at NAU for providing valuable suggestions for

field experiments and data analysis. We thank researchers at the JIC and the University of Cambridge for constructive suggestions. We gratefully acknowledge the hardware support of the Zealquest Scientific Technology (Shanghai China) for the backpack LiDAR used in this research.

**Competing interests**

The authors declare no competing financial interests.

1044 **Tables**

1045 Table 1. *Cost comparison between backpack LiDAR devices, UAV airborne LiDAR, and the handheld*
1046 *laser scanning system, with brief technical specifications.*

| LiDAR system | **System costs (academic price)** | **Brief technical spec.** | **References** |
|---|---|---|---|
| Robin (backpack) | US$350,000-375,000 with TerraSoild software (2018) | VUX-1 HA scanner, 1.5-200 m eff. range, 5-10 mm accuracy (outdoor) | www.3dlasermapping.com (discontinued) |
| BMS3D-HD (backpack) | US$310,000-330,000 with BMS3D software (2021) | HDL-32 & VLP-16 scanners, 0.5-100 m eff. range, 20 mm accuracy (outdoor) | www.viametrisbusiness.com (France) |
| Pegasus (backpack) | US$330,000-360,000 with local software (2021) | Dual VLP-16 scanner, 80 m eff. range, 10-30 mm accuracy (outdoor) | www.leica-geosystems.com (Switzerland) |
| GeoSLAM (backpack) | US$300,000-320,000 with ORBIT software (2020) | Dual ZEB Discovery scanner, 100 m eff. range, 10-30 mm accuracy (outdoor) | geoslam.com (UK) |
| SLAM-based (backpack) | A low-cost solution with Forest3D software (2020) | Dual Velodyne Puck VLP-16 sensors, 100 m eff. range, 30 mm accuracy | (Su et al., 2020) velodynelidar.com (US) |
| Airborne LiDAR | US$125,000-150,000 with SpatialExplorer (2021) | SCOUT and RANGER series, 100 m range, 50-55 mm accuracy | www.phoenixlidar.com (US) |
| Handheld LiDAR | US$25,000-50,000 with GeoSLAM Hub & Draw software (2021) | ZEB-Horizon scanner, 100 m eff. range, 10-30 mm accuracy | geoslam.com (UK) |

1047

1048

1049 **Table 2.** *Soil nutrient (0-25 cm soil layer) content before drilling in the 2019/2020 season*

| pH | Organic matter (g/kg) | $NO_3$-N (mg/kg) | Phosphate (g/kg) | Potassium (g/kg) | Total organic N (mg/kg) | Plant available Phosphate (mg/kg) | Plant available Potassium (mg/kg) |
|---|---|---|---|---|---|---|---|
| 6 | 24.2 | 1.35 | 0.61 | 13.2 | 10.4 | 3.04 | 160 |

1050
1051
1052

1053 **Table 3.** *Processing time for three types of point cloud files at each analysis step*

| Analysis steps | Processing time (backpack) | Display time (backpack) | Proc. time (UAV) | Disp. time (UAV) | Proc. time (gantry) | Dis. time (gantry) |
|---|---|---|---|---|---|---|
| *Step 1* | 2.5-3 minutes | 35-45 seconds | 1.5-2 mins | 25-30 seconds | N/A | N/A |
| *Step 2* | 1.5-2 mins | 50-60 sec. | 30-40 sec. | 40-50 sec. | N/A | N/A |
| *Step 3* | 10-15 sec. | 0.2-0.5 sec. | 30-40 sec. | 0.5-1 sec. | 10-15 sec. | 0.3-0.5 sec. |
| *Step 4* | 0.5-1.5 sec. | 0.3-1 sec. | 0.5-1 sec. | 0.5-1 sec. | 0.5-1.5 sec. | 0.5-1 sec. |
| *Step 5* | 30-40 sec. | 0.5-1.5 sec. | 20-25 sec. | 0.5-1 sec. | 5-10 sec. | 0.5-1 sec. |
| *Step 6* | 5-6 sec. | N/A | 3-4 sec. | N/A | 1-2 sec. | N/A |
| *Step 7* | 5-10 sec. per plot | N/A | 4-6 sec./plot | N/A | N/A | N/A |

1054
1055

## Figure Legends

**Figure 1: The data acquisition procedure using a backpack LiDAR device together with raw point cloud data generated through pre-processing a LiDAR-acquired 3D point cloud file.**

(**a**) An overhead orthomosaic image of the field trial area showing 486 six-metre winter wheat varieties with three levels of nitrogen (N) fertilisation treatments (i.e. 0, 180, and 270 kg N $ha^{-1}$). Red arrows represent the grid-style mapping method carried out by a LiDAR operator outside the plots. (**b**) The backpack LiDAR device (ROBIN Precision) and a real-time kinematic (RTK) base station used for 3D field phenotyping. (**c**) A high-level workflow of the pre-processing software used to generate RTK-tagged point cloud data collected by the backpack LiDAR. (**d**) The raw point clouds generated for the trial area. (**e**) Initial height-based analysis with uncalibrated 3D points, which were coloured according to z values, and example plot-level images using raw 3D points, height values, and triangle mesh.

**Figure 2: A high-level analysis pipeline established for processing LiDAR-acquired point clouds and measuring yield-related traits in 3D.**

(**a**) Select a pre-processed point cloud file (in LAS format). (**b**) Remove outliers (coloured red) in the point cloud, followed by filtering methods to differentiate ground-based terrain (e.g. soil level below the crop) and above-ground (crops) 3D points. (**c**) Generate a 2D canopy height model (CHM) and define the region of interest (ROI, denoted by the four red markers) using geo-coordinates collected by the ground-based real-time kinematic (RTK) station. (**d & e**) Detect horizontal and vertical edges using the Sobel operator, followed by the application of 2D Hough transform to produce a binary mask to segment plots in the field experiments. (**f**) Measure and export 3D trait analysis results for each plot, including measured traits (CSV), processed images (JPG), and processed point cloud (LAS).

**Figure 3: The graphical user interface (GUI) for CropQuant-3D designed for processing 3D point cloud files using 2D/3D image analysis algorithms and mathematic transformation for analysing canopy structural traits in 3D.**

(**a**) The initial GUI window of CropQuant-3D. (**b**) The GUI window after accomplishing all required analysis steps, with the progress bar showing 100%. (**c**) The intermediate results that can be displayed for each processing step integrated in the analysis procedure for processing point cloud files generated by the backpack LiDAR, including optional input parameters such as the number of rows and columns of the experimental field that users could enter to assist the algorithm for segmenting plots. (**d**) The intermediate results that can be displayed for processing point cloud files collected by unmanned aerial vehicle (UAV) aerial imaging. (**e**) The intermediate results that can be displayed for processing point cloud files generated by a gantry-mounted LiDAR system, FieldScan$^{TM}$.

**Figure 4: The pseudo-coloured uncalibrated height maps, 3D visualisation, and pseudo-coloured calibrated height maps of nitrogen use efficiency (NUE) wheat experiments under three different levels of nitrogen (N) treatments.**

(**a**) The 2D Canopy Height Model (CHM) image (to the left) and 3D digital surface model (DSM) image, created using the real-time kinematic (RTK) tagged altitude height values, and the calibrated height maps (to the right), showing the average height value of the highest 10% 3D points ($H_{10}$) for the low-N treatment; (**b & c**) the 2D CHM, 3D DSM (left) and the calibrated height (right) images for the medium-N and high-N treatments. The unified height scale bar for the three sub-figures is shown.

**Figure 5: The analysis process of measuring 3D canopy surface area and canopy coverage at the plot level using voxels and triangular mesh for wheat varieties.**

(**a**) 3D points for the canopy region using the highest 50% points ($H_{50}$) in a given plot. (**b**) $H_{50}$ points projected onto the ground plane, generating pixels representing crop canopy regions, which were processed by an adaptive approach to calculate the normalised canopy coverage trait (0-1, where 1 stands for 100%). (**c**) A brief analysis process of computing the 3D surface area trait using triangle

mesh. (**d**) The normalised 3D surface results (0-1, where 1 stands for maximum 3D surface area in a given plot) of a wheat variety under three nitrogen treatments.

**Figure 6: The analysis procedure of measuring 3D canopy structure at the plot level using 2D CHM images and a 2D discrete Fourier transform (DFT), resulting in 3D canopy structural curves for separating variety responses to different nitrogen (N) treatments.**

(**a**) The pseudo-coloured height images and their associated grayscale height images (intensity values correspond to height values) in a plot, under three N treatments. (**b**) Frequency spectrograms generated using 2D DFT of the grayscale height images, containing all frequencies of height values and their magnitude in the plot. (**c**) Centralised magnitude of DFT produced to enable frequency and amplitude sampling through red coloured lines on the diagonal of the image; regular patterns observable in the images with medium- and high-N treatments. (**d**) Three canopy structural curves plotted to present structural differences together with cross-sections of 3D points at the canopy level, showing the wheat variety's different responses to three N treatments as well as the procedure of computing 3D canopy index (3DCI; 0-1, where 1 stands for maximum accumulated spatial variation in a given plot) based on the curves and areas beneath the curves.

**Figure 7: The square of the correlation coefficient ($R^2$) calculated to evaluate correlations between height estimates, canopy surface area and 3D canopy index (3DCI) computed by CropQuant-3D and manual measurements in the 2019/20 field trial, at three different levels of nitrogen (N) fertilisation; *p*-values computed through the linear regression analysis also reported.**

(**a**) Plot-based correlation analysis of the peak height measured by CropQuant-3D and manual height measurements. (**b**) Variety-based correlation analysis of the peak height measured by CropQuant-3D and manual height measurements. (**c**) Correlation analysis of the 3D surface area index and the grain number per unit area (GN $m^{-2}$) data. (**d**) Correlation analysis between 3DCI and spike numbers per square metre (SN $m^{-2}$). Plot means (a) and genotype means (b) are shown.

**Figure 8: A case study of classifying wheat varieties' nitrogen responses using the 3D canopy index (3DCI) and spike number per unit area for 11 varieties from the Zhenmai and Ningmai collections under three nitrogen (N) application levels. Error bars used in the spike number per metre square (SN $m^{-2}$) scores represent one standard error.**

(**a**) The first N response class, showing canopy structural curves of ZM-4 and the associated spike number per metre square (SN $m^{-2}$) scores under the three nitrogen (N) treatments. Also in this class were varieties NMzi-1019, ZM-5 and ZM-1 (see **Fig. 6** for the explanation of the measure). (**b**) The second N response class, showing canopy structural curves of NMzi-1 and the associated SN $m^{-2}$ scores under the three N treatments. Also in this class were NMzi-1, ZM-10 and ZM-12. (**c**) The third N response class, showing canopy structural curves of NM-26 and the associated SN $m^{-2}$ scores under the three N treatments. Also in this class was ZM-8. (**d**) The fourth N response class, showing canopy structural curves of ZM-168 and the associated SN $m^{-2}$ scores under the three N treatments. Also in this class was line ZM-09196. Values shown in corresponding colour next to each curve in the plots are computed 3DCI values.

**Figure 9: A performance matrix to evaluate nitrogen use efficiency (NUE) of wheat varieties using traits and measures for 11 wheat varieties from the Zhenmai and Ningmai collections under three nitrogen (N) applications.**

(**a-c**) A range of canopy measures (i.e. 3DCI and canopy surface area index), plot level height, and key yield components, i.e. spike number per metre square (SN $m^{-2}$) and grain number per metre square (GN $m^{-2}$), combined to assess winter wheat varieties under three N treatments, with 15% over the trimmed mean coloured dark orange, 7.5~15% coloured light orange, -7.5~7.5% coloured yellow, -15~-7.5% coloured light blue, and -15% below the trimmed mean coloured dark blue. Selected varieties were coloured red, indicating they were ranked higher than the other varieties by the performance matrix.

## References

**An N, Palmer CM, Baker RL, Markelz RJC, Ta J, Covington MF, Maloof JN, Welch SM, Weinig C** (2016) Plant high-throughput phenotyping using photogrammetry and imaging techniques to measure leaf length and rosette area. Comput Electron Agric **127**: 376–394

**Antonarakis AS, Richards KS, Brasington J, Muller E** (2010) Determining leaf area index and leafy tree roughness using terrestrial laser scanning. Water Resour Res **46**: 1–12

**Araus JL, Cairns JE** (2014) Field high-throughput phenotyping: the new crop breeding frontier. Trends Plant Sci **19**: 52–61

**Arnó J, Escolà A, Vallès JM, Llorens J, Sanz R, Masip J, Palacín J, Rosell-Polo JR** (2013) Leaf area index estimation in vineyards using a ground-based LiDAR scanner. Precis Agric **14**: 290–306

**Barker J, Zhang N, Sharon J, Steeves R, Wang X, Wei Y, Poland J** (2016) Development of a field-based high-throughput mobile phenotyping platform. Comput Electron Agric **122**: 74–85

**Bauer A, Bostrom AG, Ball J, Applegate C, Cheng T, Laycock S, Rojas SM, Kirwan J, Zhou J** (2019) Combining computer vision and deep learning to enable ultra-scale aerial phenotyping and precision agriculture: A case study of lettuce production. Hortic Res **6**: 1–12

**Bucksch A, Lindenbergh RC, Menenti M** (2009) SkelTre-fast skeletonisation for imperfect point cloud data of botanic trees. *In* R Veltkamp, ed, Eurographics Work. 3D Object Retr. pp 1–8

**Burnette M, Rohde GS, Fahlgren N, Sagan V, Sidike P, Kooper R, Terstriep JA, Mockler T, Andrade-Sanchez P, Ward R, et al** (2018) TERRA-REF data processing infrastructure. ACM IPEARC 18. ACM, Pittsburgh, pp 1–7

**Butler H, Chambers B, Hartzell P, Glennie C** (2020) PDAL: An open source library for the processing and analysis of point clouds. Comput Geosci **Dec**: 104680

**Cabrera-Bosquet L, Fournier C, Brichet N, Welcker C, Suard BB, Tardieu F** (2016) High-throughput estimation of incident light, light interception and radiation-use efficiency of thousands of plants in a phenotyping platform. New Phytol **212**: 269–281

**Carpenter AE, Kamentsky L, Eliceiri KW** (2012) A call for bioimaging software usability. Nat Methods **9**: 666–70

**Cendrero-Mateo MP, Muller O, Albrecht H, Burkart A, Gatzke S, Janssen B, Keller B, Körber N, Kraska T, Matsubara S, et al** (2017) Field Phenotyping: Challenges and Opportunities. Terr. Ecosyst. Res. Infrastructures. pp 53–80

**Cobb JN, DeClerck G, Greenberg A, Clark R, McCouch S** (2013) Next-generation phenotyping: Requirements and strategies for enhancing our understanding of genotype-phenotype relationships and its relevance to crop improvement. Theor Appl Genet **126**: 867–887

**Colmer J, O'Neill CM, Wells R, Bostrom A, Reynolds D, Websdale D, Shiralagi G, Lu W, Lou Q, Le Cornu T, et al** (2020) SeedGerm: a cost-effective phenotyping platform for automated seed imaging and machine-learning based phenotypic analysis of crop seed germination. New Phytol **228**: 778–793

**Cooley JW, Tukey JW** (1965) An Algorithm for the Machine Calculation of Complex Fourier Series. Math Comput **19**: 297

**Crain JL, Wei Y, Barker J, Thompson SM, Alderman PD, Reynolds M, Zhang N, Poland J** (2016) Development and deployment of a portable field phenotyping platform. Crop Sci **56**: 965–975

**Deery D, Jimenez-Berni J, Jones H, Sirault X, Furbank R** (2014) Proximal Remote Sensing Buggies and Potential Applications for Field-Based Phenotyping. Agronomy **4**: 349–379

**Deery DM, Rebetzke GJ, Jimenez-Berni JA, Condon AG, Smith DJ, Bechaz KM, Bovill WD** (2020) Ground-Based LiDAR Improves Phenotypic Repeatability of Above-Ground Biomass and Crop Growth Rate in Wheat. Plant Phenomics **2020**: 1–11

**Duan T, Chapman SC, Holland E, Rebetzke GJ, Guo Y, Zheng B** (2016) Dynamic quantification of canopy structure to characterize early plant vigour in wheat genotypes. J Exp Bot **67**: 4523–4534

**Duan T, Zheng B, Guo W, Ninomiya S, Guo Y, Chapman SC, A TD, A BZ, C WG, C SN, et al** (2017) Comparison of ground cover estimates from experiment plots in cotton, sorghum and sugarcane based on images and ortho-mosaics captured by UAV. Funct Plant Biol **44**: 169–183

**Duda RO, Hart PE** (1972) Use of the Hough Transformation to Detect Lines and Curves in Pictures. Commun ACM **15**: 11–15

**Edelsbrunner H, Kirkpatrick D, Seidel R** (1983) On the shape of a set of points in the plane. IEEE Trans Inf theory **29**: 551–559

**Feng W, Yao X, Zhu Y, Tian YC, Cao WX** (2008) Monitoring leaf nitrogen status with hyperspectral reflectance in wheat. Eur J Agron **28**: 394–404

**Fiorani F, Schurr U** (2013) Future scenarios for plant phenotyping. Annu Rev Plant Biol **64**: 267–91

**Firdousi R, Parveen S** (2014) Local Thresholding Techniques in Image Binarization. Int J Eng Comput Sci **3**: 4062–4065

**Friedli M, Kirchgessner N, Grieder C, Liebisch F, Mannale M, Walter A** (2016) Terrestrial 3D laser scanning to track the increase in canopy height of both monocot and dicot crop species under field conditions. Plant Methods **12**: 1–15

**Fritsche-Neto R, Borém A** (2015) Phenomics: how next-generation phenotyping is revolutionazing plant breeding. doi: 10.1007/978-3-319-13677-6

**Furbank RT, Jimenez-Berni JA, George-Jaeggli B, Potgieter AB, Deery DM** (2019) Field crop phenomics: enabling breeding for radiation use efficiency and biomass in cereal crops. New Phytol **223**: 1714–1727

**Furbank RT, Tester M** (2011) Phenomics - technologies to relieve the phenotyping bottleneck. Trends Plant Sci **16**: 635–44

**Girardeau-Montaut D** (2015) CloudCompare - User manual v2.6.1. Stuttgart, Germany

**Godwin RJ, Wood GA, Taylor JC, Knight SM, Welsh JP** (2003) Precision farming of cereal crops: A review of a six year experiment to develop management guidelines. Biosyst Eng **84**: 375–391

**Good AG, Shrawat AK, Muench DG** (2004) Can less yield more? Is reducing nutrient input into the environment compatible with maintaining crop production? Trends Plant Sci **9**: 597–605

**Green CF., Dawkins TCK., Hunter B** (1985) Influence of foliar applied chlormequat on radiation attenuation by winter barley canopies. J Agric Sci **105**: 213–216

**Griffiths S, Simmonds J, Leverington M, Wang Y, Fish L, Sayers L, Alibert L, Orford S, Wingen L, Snape J** (2012) Meta-QTL analysis of the genetic control of crop height in elite European winter wheat germplasm. Mol Breed **29**: 159–171

**Griffiths S, Wingen L, Pietragalla J, Garcia G, Hasan A, Miralles D, Calderini DF,**

**Ankleshwaria JB, Waite ML, Simmonds J, et al** (2015) Genetic dissection of grain size and grain number trade-offs in CIMMYT wheat germplasm. PLoS One **10**: 1–18

**Guo Q, Wu F, Pang S, Zhao X, Chen L, Liu J, Xue B, Xu G, Li L, Jing H, et al** (2018) Crop 3D—a LiDAR based platform for 3D high-throughput crop phenotyping. Sci China Life Sci **61**: 328–339

**Haralick R, Shanmugan K, Dinstein I** (1973) Textural features for image classification. IEEE Trans Syst Man Cybern **3**: 610–621

**Harkel J ten, Bartholomeus H, Kooistra L** (2020) Biomass and Crop Height Estimation of Different Crops Using UAV-Based Lidar. Remote Sens **12**: 1–18

**Hirafuji M, Yoichi H** (2011) Creating high-performance/low-cost ambient sensor cloud system using OpenFS (Open Field Server) for high-throughput phenotyping. … 2011 Proc. pp 2090–2092

**Holman FH, Riche AB, Castle M, Wooster MJ, Hawkesford MJ** (2019) Radiometric Calibration of 'Commercial off the Shelf' Cameras for UAV-Based High-Resolution Temporal Crop Phenotyping of Reflectance and NDVI. Remote Sens **11**: 1657

**Holman FH, Riche AB, Michalski A, Castle M, Wooster MJ, Hawkesford MJ** (2016) High throughput field phenotyping of wheat plant height and growth rate in field plot trials using UAV based remote sensing. Remote Sens **8**: 1–24

**Hosoi F, Omasa K** (2009) Estimating vertical plant area density profile and growth parameters of a wheat canopy at different growth stages using three-dimensional portable lidar imaging. ISPRS J Photogramm Remote Sens **64**: 151–158

**Howse J** (2013) OpenCV Computer Vision with Python, 1st ed. Packt Publishing Ltd., Birmingham, UK

**Hyyppä E, Yu X, Kaartinen H, Hakala T, Kukko A, Vastaranta M, Hyyppä J** (2020) Comparison of backpack, handheld, under-canopy UAV, and above-canopy UAV laser scanning for field reference data collection in boreal forests. Remote Sens **12**: 1–31

**Jimenez-Berni JA, Deery DM, Rozas-Larraondo P, Condon ATG, Rebetzke GJ, James RA, Bovill WD, Furbank RT, Sirault XRR** (2018) High throughput determination of plant height, ground cover, and above-ground biomass in wheat with LiDAR. Front Plant Sci **9**: 1–18

**Jin S, Su Y, Wu F, Pang S, Gao S, Hu T, Liu J, Guo Q** (2019) Stem-Leaf Segmentation and Phenotypic Trait Extraction of Individual Maize Using Terrestrial LiDAR Data. IEEE Trans Geosci Remote Sens **57**: 1336–1346

**Jin S, Sun X, Wu F, Su Y, Li Y, Song S, Xu K, Ma Q, Baret F, Jiang D, et al** (2021) Lidar sheds new light on plant phenomics for plant breeding and management: Recent advances and future prospects. ISPRS J Photogramm Remote Sens **171**: 202–223

**Kachamba DJ, Ørka HO, Gobakken T, Eid T, Mwase W** (2016) Biomass estimation using 3D data from unmanned aerial vehicle imagery in a tropical woodland. Remote Sens **8**: 1–18

**Kelly D, Vatsa A, Mayham W, Ng L, Thompson A, Kazic T** (2016) An opinion on imaging challenges in phenotyping field crops. Mach Vis Appl **27**: 681–694

**Kirchgessner N, Liebisch F, Yu K, Pfeifer J, Friedli M, Hund A, Walter A** (2017) The ETH field phenotyping platform FIP: A cable-suspended multi-sensor system. Funct Plant Biol **44**: 154–168

**Korzeniowska K, Łącka M** (2011) Generating dem from lidar data – comparison of available software tools. Arch Photogramm Cartogr Remote Sens **22**: 271–284

**Kroon D-J** (2009) NUMERICAL OPTIMIZATION OF KERNEL BASED IMAGE DERIVATIVES Dirk-Jan Kroon University of Twente , Enschede. Area

**Langer RHM, Liew FKY** (1973) Effects of varying nitrogen supply at different stages of the reproductive phase on spikelet and grain production and on grain nitrogen in wheat. Aust J Agric Res **24**: 647–656

**Li M, Shao MR, Zeng D, Ju T, Kellogg EA, Topp CN** (2020a) Comprehensive 3D phenotyping reveals continuous morphological variation across genetically diverse sorghum inflorescences. New Phytol **226**: 1873–1885

**Li P, Zhang X, Wang W, Zheng H, Yao X, Tian Y, Zhu Y, Cao W, Chen Q, Cheng T** (2020b) Estimating aboveground and organ biomass of plant canopies across the entire season of rice growth with terrestrial laser scanning. Int J Appl Earth Obs Geoinf **91**: 102132

**Li W, Niu Z, Huang N, Wang C, Gao S, Wu C** (2015) Airborne LiDAR technique for estimating biomass components of maize: A case study in Zhangye City, Northwest China. Ecol Indic **57**:

1301 486–496
1302 **Lin Y** (2015) LiDAR: An important tool for next-generation phenotyping technology of high
1303 potential for plant phenomics? Comput Electron Agric **119**: 61–73
1304 **Lindsay JB** (2016) Whitebox GAT: A case study in geomorphometric analysis. Comput Geosci. doi:
1305 10.1016/j.cageo.2016.07.003
1306 **Lobet G** (2017) Image Analysis in Plant Sciences: Publish Then Perish. Trends Plant Sci **22**: 559–566
1307 **Lowe DG** (2004) Distinctive Image Features from Scale-Invariant Keypoints. Int J Comput Vis **60**:
1308 91–110
1309 **Masiero A, Fissore F, Guarnieri A, Pirotti F, Visintini D, Vettore A** (2018) Performance
1310 evaluation of two indoor mapping systems: Low-Cost UWB-aided photogrammetry and
1311 backpack laser scanning. Appl Sci **8**: 1–19
1312 **Mezirow J** (1978) Perspective transformation. Adult Educ Q **28**: 100–110
1313 **Momen M, Campbell MT, Walia H, Morota G** (2019) Predicting longitudinal traits derived from
1314 high-throughput phenomics in contrasting environments using genomic Legendre polynomials
1315 and B-splines. G3 Genes, Genomes, Genet **9**: 3369–3380
1316 **Naito H, Ogawa S, Valencia MO, Mohri H, Urano Y, Hosoi F, Shimizu Y, Chavez AL, Ishitani**
1317 **M, Selvaraj MG, et al** (2017) Estimating rice yield related traits and quantitative trait loci
1318 analysis under different nitrogen treatments using a simple tower-based field phenotyping
1319 system with modified single-lens reflex cameras. ISPRS J Photogramm Remote Sens **125**: 50–
1320 62
1321 **Nguyen GN, Kant S** (2018) Improving nitrogen use efficiency in plants: Effective phenotyping in
1322 conjunction with agronomic and genetic approaches. Funct Plant Biol **45**: 606–619
1323 **Omasa K, Hosoi F, Konishi A** (2007) 3D lidar imaging for detecting and understanding plant
1324 responses and canopy structure. J Exp Bot **58**: 881–898
1325 **Panjvani K, Dinh A V., Wahid KA** (2019) LiDARPheno – A low-cost LiDAR-based 3D scanning
1326 system for leaf morphological trait extraction. Front Plant Sci. doi: 10.3389/fpls.2019.00147
1327 **Pask A, Pietragalla J, Mullan D, Reynolds M** (2012) Physiological Breeding II: A Field Guide to
1328 Wheat Phenotyping. CIMMYT. doi: 10.1017/CBO9781107415324.004

**Paulus S** (2019) Measuring crops in 3D: Using geometry for plant phenotyping. Plant Methods **15**: 1–13

**Pieruschka R, Schurr U** (2019) Plant Phenotyping: Past, Present, and Future. Plant Phenomics **2019**: 1–6

**Power JF, Alessi J** (1978) Tiller development and yield of standard and semidwarf spring wheat varieties as affected by nitrogen fertilizer. J Agric Sci **90**: 97–108

**Powlson D, Norse D, Chadwick D, Lu Y, Zhang W, Zhang F** (2014) Contribution of improved nitrogen fertilizer use to development of a low carbon economy in China. World Agric **4**: 10–18

**Raun WR, Johnson GV** (1999) Improving nitrogen use efficiency for cereal production. Agron J **91**: 357–363

**Raybould A, Quemada H** (2010) Bt crops and food security in developing countries: Realised benefits, sustainable use and lowering barriers to adoption. Food Secur **2**: 247–259

**Reynolds D, Ball J, Bauer A, Davey R, Griffiths S, Zhou J** (2019a) CropSight: A scalable and open-source information management system for distributed plant phenotyping and IoT-based crop management. Gigascience **8**: 1–11

**Reynolds D, Baret F, Welcker C, Bostrom A, Ball J, Cellini F, Lorence A, Chawade A, Khafif M, Noshita K, et al** (2019b) What is cost-efficient phenotyping? Optimizing costs for different scenarios. Plant Sci **282**: 14–22

**Reynolds M, Langridge P** (2016) Physiological breeding. Curr Opin Plant Biol **31**: 162–171

**Ritter N, Ruth M** (1997) The GeoTIFF data interchange standard for raster geographic images. Int J Remote Sens **18**: 1637–1647

**Roitsch T, Cabrera-Bosquet L, Fournier A, Ghamkhar K, Jiménez-Berni J, Pinto F, Ober ES** (2019) Review: New sensors and data-driven approaches—A path to next generation phenomics. Plant Sci **282**: 2–10

**Roussel JR, Auty D, Coops NC, Tompalski P, Goodbody TRH, Meador AS, Bourdon JF, de Boissieu F, Achim A** (2020) lidR: An R package for analysis of Airborne Laser Scanning (ALS) data. Remote Sens Environ **251**: 112061

**Roy J, Tardieu F, Tixier-Boichard M, Schurr U** (2017) European infrastructures for sustainable

agriculture. Nat Plants **3**: 756–758

**Sadras VO, Richards RA** (2014) Improvement of crop yield in dry environments: Benchmarks, levels of organisation and the role of nitrogen. J Exp Bot **65**: 1981–1995

**Sadras VO, Slafer GA** (2012) Environmental modulation of yield components in cereals: Heritabilities reveal a hierarchy of phenotypic plasticities. F Crop Res **127**: 215–224

**Sauvola J, Pietikäinen M** (2000) Adaptive document image binarization. Pattern Recognit **33**: 225–236

**Scharr H, Dee H, French AP, Tsaftaris SA** (2016) Special issue on computer vision and image analysis in plant phenotyping. Mach Vis Appl **27**: 607–609

**Shearman VJ, Scott RK, Foulkes MJ** (2005) Crop Physiology and Metabolism. Physiological Processes Associated with Wheat Yield Progress in the UK. Crop Sci **185**: 175–185

**Singh TR, Roy S, Singh OI, Sinam T, Singh KM** (2012) A New Local Adaptive Thresholding Technique in Binarization. Int J Comput Sci Issues **8**: 271–277

**Stovall AEL, Vorster AG, Anderson RS, Evangelista PH, Shugart HH** (2017) Non-destructive aboveground biomass estimation of coniferous trees using terrestrial LiDAR. Remote Sens Environ **200**: 31–42

**Su Y, Guo Q, Jin S, Guan H, Sun X, Ma Q, Hu T, Wang R, Li Y** (2020) The Development and Evaluation of a Backpack LiDAR System for Accurate and Efficient Forest Inventory. IEEE Geosci Remote Sens Lett 1–5

**Su Y, Wu F, Ao Z, Jin S, Qin F, Liu B, Pang S, Liu L, Guo Q** (2019) Evaluating maize phenotype dynamics under drought stress using terrestrial lidar. Plant Methods **15**: 1–16

**Summerfield M** (2015) Rapid GUI Programming with Python and Qt: The Definitive Guide to PyQt Programming. Pearson, London, UK

**Sun S, Li C, Paterson AH, Jiang Y, Xu R, Robertson JS, Snider JL, Chee PW** (2018) In-field high throughput phenotyping and cotton plant growth analysis using LiDAR. Front Plant Sci **9**: 1–17

**Susan S, Hanmandlu M** (2013) A non-extensive entropy feature and its application to texture classification. Neurocomputing **120**: 214–225

**Swarbreck SM, Wang M, Wang Y, Kindred D, Sylvester-Bradley R, Shi W, Varinderpal-Singh, Bentley AR, Griffiths H** (2019) A Roadmap for Lowering Crop Nitrogen Requirement. Trends Plant Sci **24**: 892–904

**Sylvester-Bradley R, Kindred DR** (2009) Analysing nitrogen responses of cereals to prioritize routes to the improvement of nitrogen use efficiency. J Exp Bot **60**: 1939–1951

**Tardieu F, Cabrera-Bosquet L, Pridmore T, Bennett M** (2017) Plant Phenomics, From Sensors to Knowledge. Curr Biol **27**: R770–R783

**Truong-Hong L, Laefer DF, Hinks T, Carr H** (2013) Combining an angle criterion with voxelization and the flying voxel method in reconstructing building models from LiDAR data. Comput Civ Infrastruct Eng **28**: 112–129

**Ubbens J, Cieslak M, Prusinkiewicz P, Stavness I** (2018) The use of plant models in deep learning: An application to leaf counting in rosette plants. Plant Methods **14**: 1–10

**UN Food & Agriculture Organization** (2009) How to Feed the World in 2050. *In* FAO, ed, Proc. High-Level Expert Forum How to Feed World 2050. UN FAO, Rome, p 733

**Vadez V, Kholová J, Hummel G, Zhokhavets U, Gupta SK, Hash CT** (2015) LeasyScan: A novel concept combining 3D imaging and lysimetry for high-throughput phenotyping of traits controlling plant water budget. J Exp Bot **66**: 5581–5593

**Valluru R, Reynolds MP, Davies WJ, Sukumaran S** (2017) Phenotypic and genome-wide association analysis of spike ethylene in diverse wheat genotypes under heat stress. New Phytol **214**: 271–283

**Virlet N, Sabermanesh K, Sadeghi-Tehran P, Hawkesford MJ, Sabermanesh P, Sadeghitehran K, Hawkesford MJ, Sabermanesh K, Sadeghi-Tehran P, Hawkesford MJ** (2017) Field Scanalyzer: An automated robotic field phenotyping platform for detailed crop monitoring. Funct Plant Biol **44**: 143–153

**Virtanen P, Gommers R, Oliphant TE, Haberland M, Reddy T, Cournapeau D, Burovski E, Peterson P, Weckesser W, Bright J, et al** (2020) SciPy 1.0: fundamental algorithms for scientific computing in Python. Nat Methods **17**: 261–272

**Van Der Walt S, Colbert SC, Varoquaux G** (2011) The NumPy array: A structure for efficient

numerical computation. Comput Sci Eng **13**: 22–30

**van der Walt S, Schönberger JL, Nunez-Iglesias J, Boulogne F, Warner JD, Yager N, Gouillart E, Yu T** (2014) Scikit-image: image processing in Python. PeerJ **2**: 1–18

**Walter JDC, Edwards J, McDonald G, Kuchel H** (2019) Estimating Biomass and Canopy Height With LiDAR for Field Crop Breeding. Front Plant Sci. doi: 10.3389/fpls.2019.01145

**Wang C, Nie S, Xi X, Luo S, Sun X** (2017) Estimating the biomass of maize with hyperspectral and LiDAR data. Remote Sens **9**: 1–12

**Ward B, Brien C, Oakey H, Pearson A, Negrão S, Schilling RK, Taylor J, Jarvis D, Timmins A, Roy SJ, et al** (2019) High-throughput 3D modelling to dissect the genetic control of leaf elongation in barley (Hordeum vulgare). Plant J **98**: 555–570

**Wu D, Guo Z, Ye J, Feng H, Liu J, Chen G, Zheng J, Yan D, Yang X, Xiong X, et al** (2019) Combining high-throughput micro-CT-RGB phenotyping and genome-wide association study to dissect the genetic architecture of tiller growth in rice. J Exp Bot **70**: 545–561

**Yang W, Feng H, Zhang X, Zhang J, Doonan JH, Batchelor WD, Xiong L, Yan J** (2020) Crop Phenomics and High-Throughput Phenotyping: Past Decades, Current Challenges, and Future Perspectives. Mol Plant **13**: 187–214

**Zadocks JC, CHANG TT, KONZAK CF** (1974) A decimal code for the growth stages of cereals. Weed Res **14**: 415–421

**Zhang H, Li Y, Zhu JK** (2018) Developing naturally stress-resistant crops for a sustainable agriculture. Nat Plants **4**: 989–996

**Zhao C, Zhang Y, Du J, Guo X, Wen W, Gu S, Wang J, Fan J** (2019) Crop phenomics: Current status and perspectives. Front Plant Sci. doi: 10.3389/fpls.2019.00714

**Zhao X, Guo Q, Su Y, Xue B** (2016) Improved progressive TIN densification filtering algorithm for airborne LiDAR data in forested areas. ISPRS J Photogramm Remote Sens **117**: 79–91

**Zhou J, Applegate C, Alonso AD, Reynolds D, Orford S, Mackiewicz M, Griffiths S, Penfield S, Pullen N** (2017a) Leaf-GP: An open and automated software application for measuring growth phenotypes for arabidopsis and wheat. Plant Methods **13**: 1–30

**Zhou J, Reynolds D, Websdale D, Le Cornu T, Gonzalez-Navarro O, Lister C, Orford S,**

**Laycock S, Finlayson G, Stitt T, et al** (2017b) CropQuant: An automated and scalable field phenotyping platform for crop monitoring and trait measurements to facilitate breeding and digital agriculture. bioRxiv 161547

**Zhou QY, Park J, Koltun V** (2018) Open3D: A modern library for 3D data processing. arXiv 1–8

**Figure 1: The data acquisition procedure using a backpack LiDAR device together with raw point cloud data generated through pre-processing a LiDAR-acquired 3D point cloud file.**

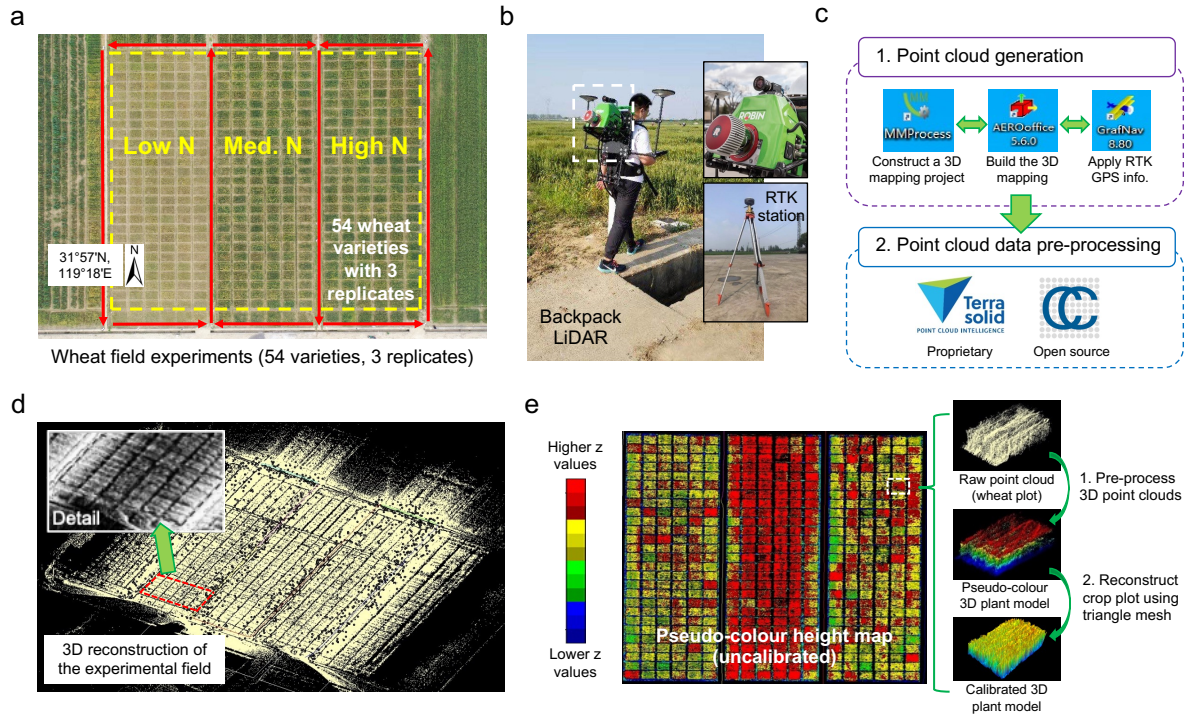


(**a**) An overhead orthomosaic image of the field trial area showing 486 six-metre winter wheat varieties with three levels of nitrogen (N) fertilisation treatments (i.e. 0, 180, and 270 kg N $ha^{-1}$). Red arrows represent the grid-style mapping method carried out by a LiDAR operator outside the plots. (**b**) The backpack LiDAR device (ROBIN Precision) and a real-time kinematic (RTK) base station used for 3D field phenotyping. (**c**) A high-level workflow of the pre-processing software used to generate RTK-tagged point cloud data collected by the backpack LiDAR. (**d**) The raw point clouds generated for the trial area. (**e**) Initial height-based analysis with uncalibrated 3D points, which were coloured according to z values, and example plot-level images using raw 3D points, height values, and triangle mesh.

**Figure 2: A high-level analysis pipeline established for processing LiDAR-acquired point clouds and measuring yield-related traits in 3D.**

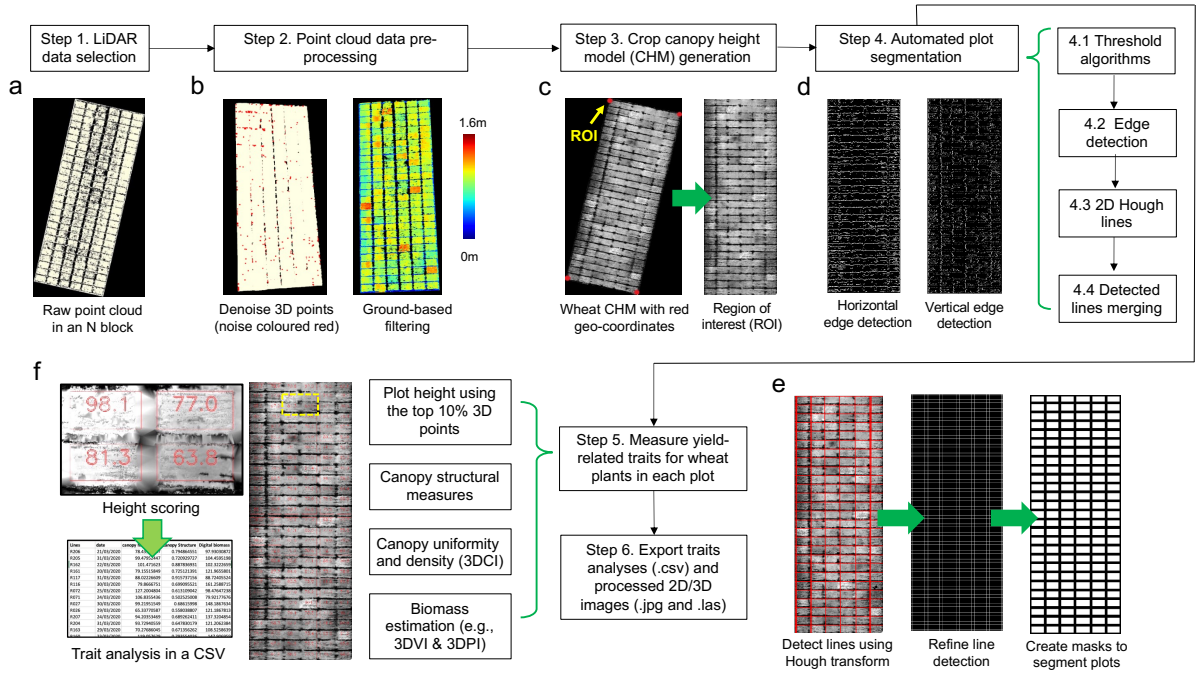


(**a**) Select a pre-processed point cloud file (in LAS format). (**b**) Remove outliers (coloured red) in the point cloud, followed by filtering methods to differentiate ground-based terrain (e.g. soil level below the crop) and above-ground (crops) 3D points. (**c**) Generate a 2D canopy height model (CHM) and define the region of interest (ROI, denoted by the four red markers) using geo-coordinates collected by the ground-based real-time kinematic (RTK) station. (**d & e**) Detect horizontal and vertical edges using the Sobel operator, followed by the application of 2D Hough transform to produce a binary mask to segment plots in the field experiments. (**f**) Measure and export 3D trait analysis results for each plot, including measured traits (CSV), processed images (JPG), and processed point cloud (LAS).

**Figure 3: The graphical user interface (GUI) for CropQuant-3D designed for processing 3D point cloud files using 2D/3D image analysis algorithms and mathematic transformation for analysing canopy structural traits in 3D.**

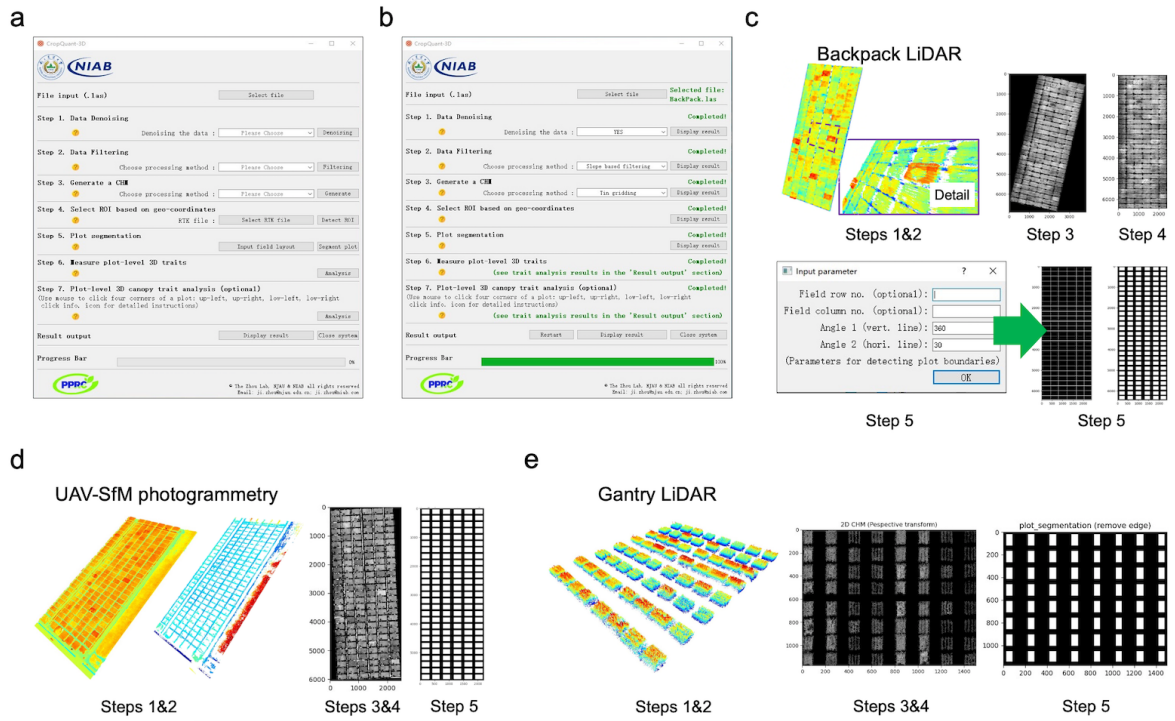


(**a**) The initial GUI window of CropQuant-3D. (**b**) The GUI window after accomplishing all required analysis steps, with the progress bar showing 100%. (**c**) The intermediate results that can be displayed for each processing step integrated in the analysis procedure for processing point cloud files generated by the backpack LiDAR, including optional input parameters such as the number of rows and columns of the experimental field that users could enter to assist the algorithm for segmenting plots. (**d**) The intermediate results that can be displayed for processing point cloud files collected by unmanned aerial vehicle (UAV) aerial imaging. (**e**) The intermediate results that can be displayed for processing point cloud files generated by a gantry-mounted LiDAR system, FieldScan$^{TM}$.

**Figure 4: The pseudo-coloured uncalibrated height maps, 3D visualisation, and pseudo-coloured calibrated height maps of nitrogen use efficiency (NUE) wheat experiments under three different levels of nitrogen (N) treatments.**

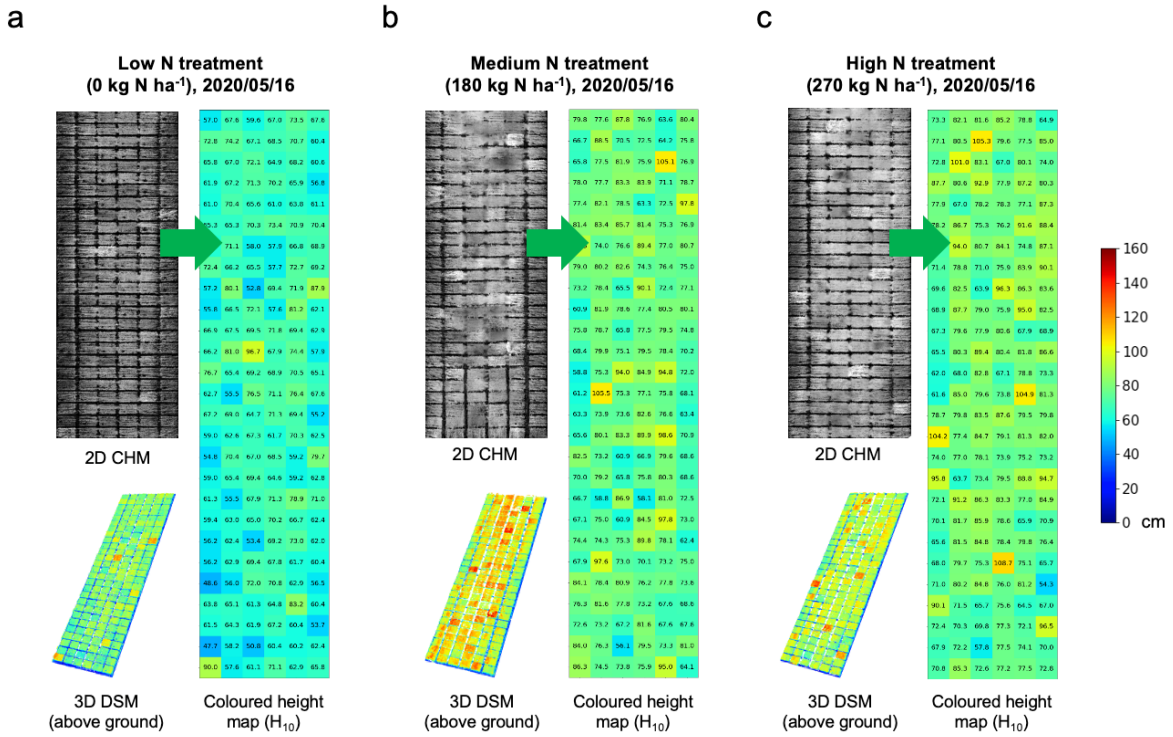


(**a**) The 2D Canopy Height Model (CHM) image (to the left) and 3D digital surface model (DSM) image, created using the real-time kinematic (RTK) tagged altitude height values, and the calibrated height maps (to the right), showing the average height value of the highest 10% 3D points ($H_{10}$) for the low-N treatment; (**b & c**) the 2D CHM, 3D DSM (left) and the calibrated height (right) images for the medium-N and high-N treatments. The unified height scale bar for the three sub-figures is shown.

**Figure 5: The analysis process of measuring 3D canopy surface area and canopy coverage at the plot level using voxels and triangular mesh for wheat varieties.**

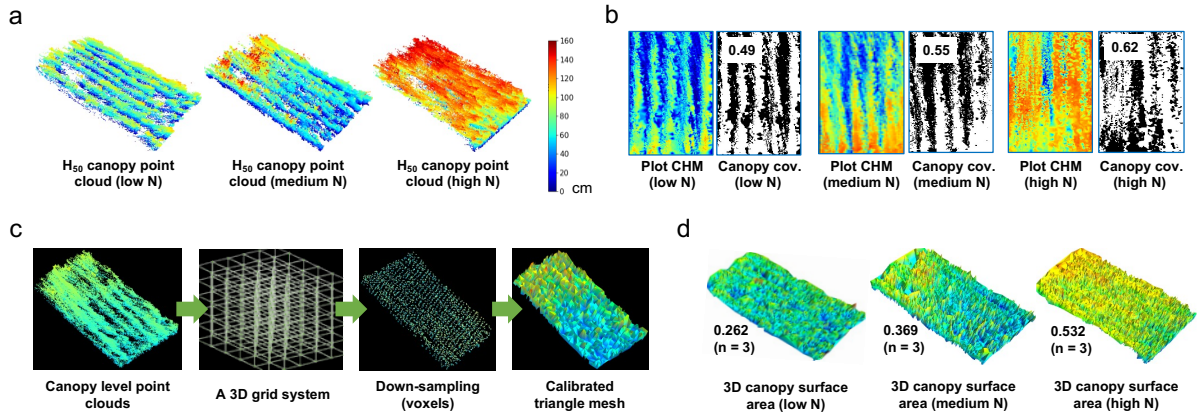


(**a**) 3D points for the canopy region using the highest 50% points ($H_{50}$) in a given plot. (**b**) $H_{50}$ points projected onto the ground plane, generating pixels representing crop canopy regions, which were processed by an adaptive approach to calculate the normalised canopy coverage trait (0-1, where 1 stands for 100%). (**c**) A brief analysis process of computing the 3D surface area trait using triangle mesh. (**d**) The normalised 3D surface results (0-1, where 1 stands for maximum 3D surface area in a given plot) of a wheat variety under three nitrogen treatments.

**Figure 6: The analysis procedure of measuring 3D canopy structure at the plot level using 2D CHM images and a 2D discrete Fourier transform (DFT), resulting in 3D canopy structural curves for separating variety responses to different nitrogen (N) treatments.**

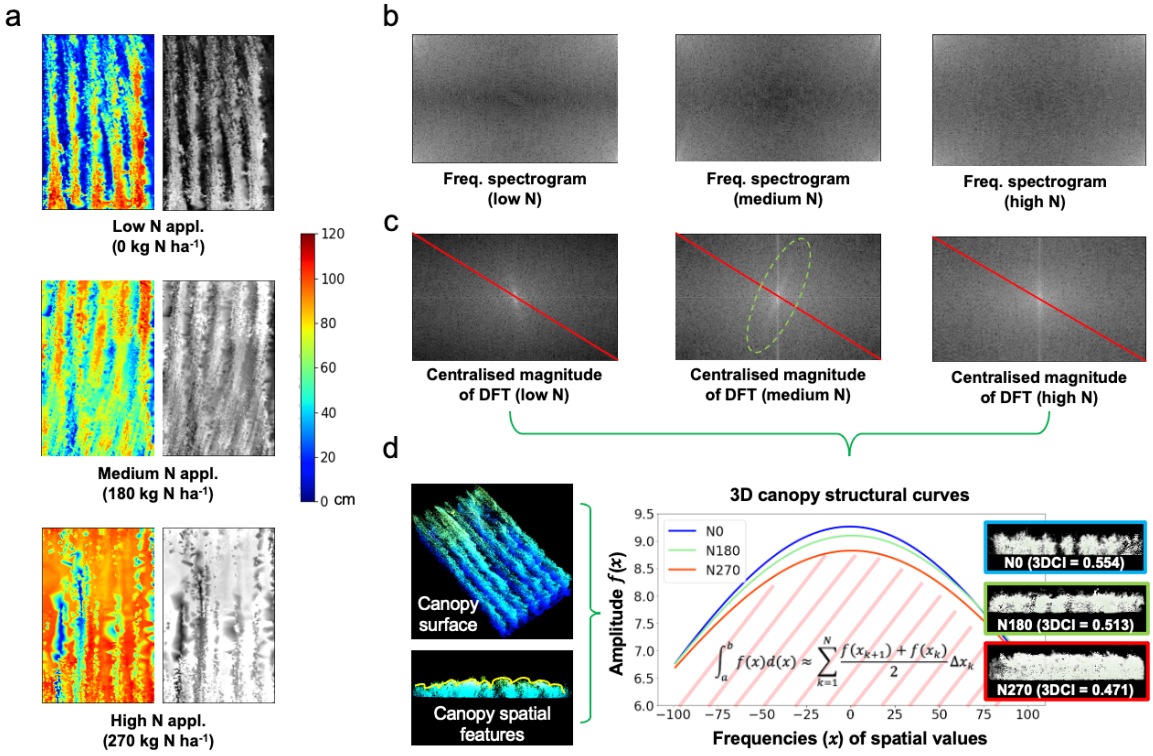


(**a**) The pseudo-coloured height images and their associated grayscale height images (intensity values correspond to height values) in a plot, under three N treatments. (**b**) Frequency spectrograms generated using 2D DFT of the grayscale height images, containing all frequencies of height values and their magnitude in the plot. (**c**) Centralised magnitude of DFT produced to enable frequency and amplitude sampling through red coloured lines on the diagonal of the image; regular patterns observable in the images with medium- and high-N treatments. (**d**) Three canopy structural curves plotted to present structural differences together with cross-sections of 3D points at the canopy level, showing the wheat variety's different responses to three N treatments as well as the procedure of computing 3D canopy index (3DCI; 0-1, where 1 stands for maximum accumulated spatial variation in a given plot) based on the curves and areas beneath the curves.

**Figure 7: The square of the correlation coefficient ($R^2$) calculated to evaluate correlations between height estimates, canopy surface area and 3D canopy index (3DCI) computed by CropQuant-3D and manual measurements in the 2019/20 field trial, at three different levels of nitrogen (N) fertilisation; *p*-values computed through the linear regression analysis also reported.**

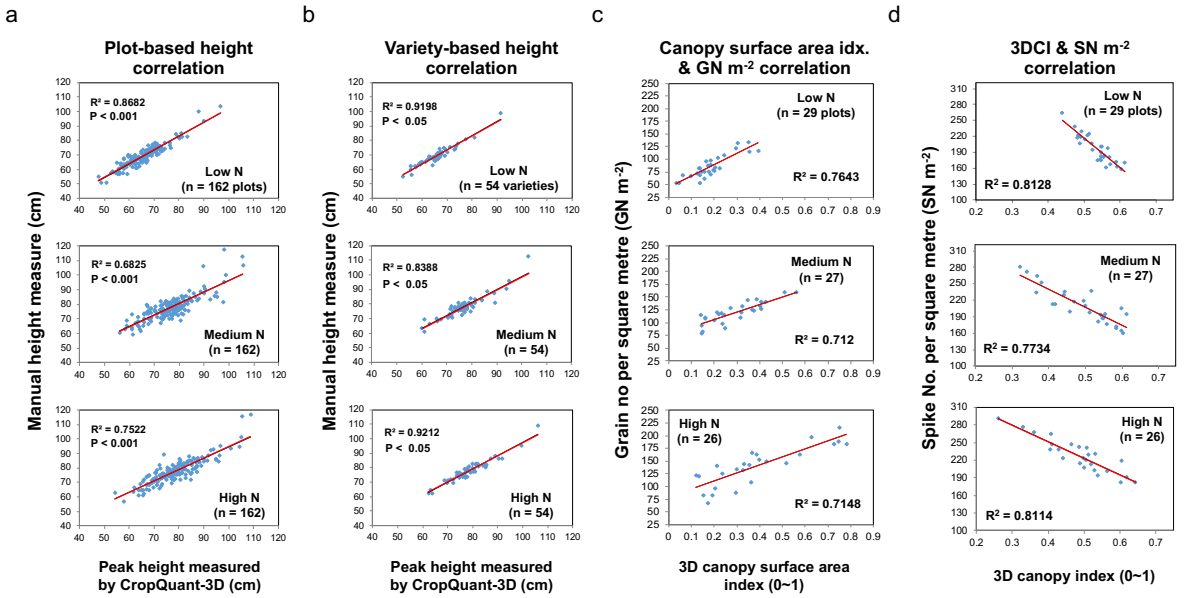


(**a**) Plot-based correlation analysis of the peak height measured by CropQuant-3D and manual height measurements. (**b**) Variety-based correlation analysis of the peak height measured by CropQuant-3D and manual height measurements. (**c**) Correlation analysis of the 3D surface area index and the grain number per unit area (GN $m^{-2}$) data. (**d**) Correlation analysis between 3DCI and spike numbers per square metre (SN $m^{-2}$). Plot means (a) and genotype means (b) are shown.

**Figure 8: A case study of classifying wheat varieties' nitrogen responses using the 3D canopy index (3DCI) and spike number per unit area for 11 varieties from the Zhenmai and Ningmai collections under three nitrogen (N) application levels. Error bars used in the spike number per metre square (SN $m^{-2}$) scores represent one standard error.**

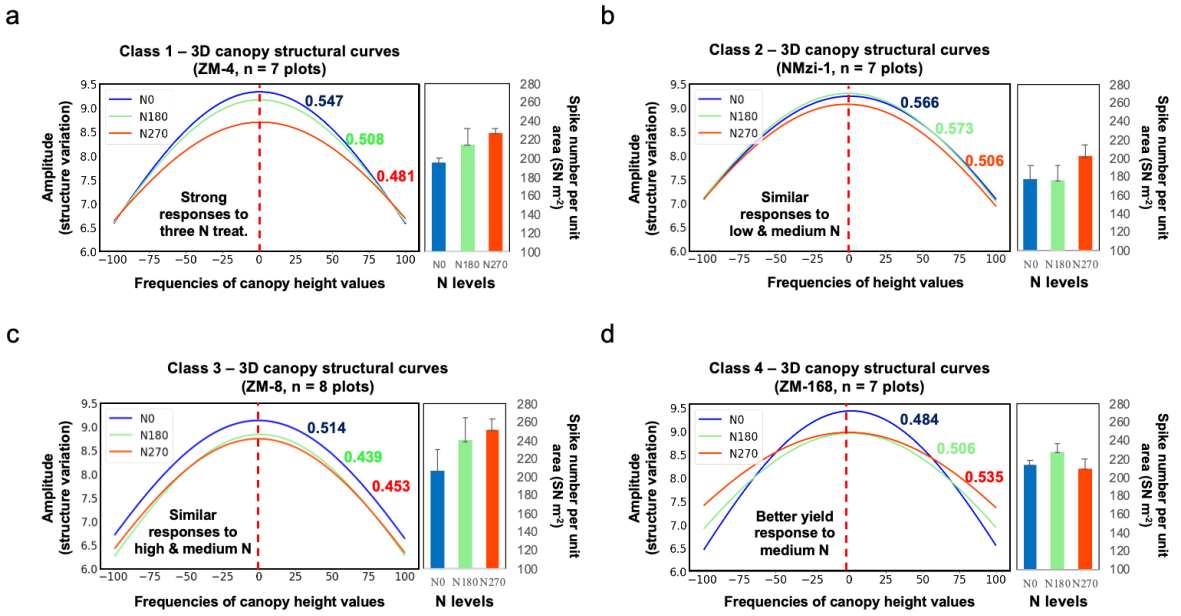


(**a**) The first N response class, showing canopy structural curves of ZM-4 and the associated spike number per metre square (SN $m^{-2}$) scores under the three nitrogen (N) treatments. Also in this class were varieties NMzi-1019, ZM-5 and ZM-1 (see **Fig. 6** for the explanation of the measure). (**b**) The second N response class, showing canopy structural curves of NMzi-1 and the associated SN $m^{-2}$ scores under the three N treatments. Also in this class were NMzi-1, ZM-10 and ZM-12. (**c**) The third N response class, showing canopy structural curves of NM-26 and the associated SN $m^{-2}$ scores under the three N treatments. Also in this class was ZM-8. (**d**) The fourth N response class, showing canopy structural curves of ZM-168 and the associated SN $m^{-2}$ scores under the three N treatments. Also in this class was line ZM-09196. Values shown in corresponding colour next to each curve in the plots are computed 3DCI values.

**Figure 9: A performance matrix to evaluate nitrogen use efficiency (NUE) of wheat varieties using traits and measures for 11 wheat varieties from the Zhenmai and Ningmai collections under three nitrogen (N) applications.**

a

**Low N (n = 29 plots, 11 varieties)**

| Lines | SN $m^{-2}$ | GW $m^{-2}$ | 3DCI | Can_Sur | Height | Overall rank |
|---|---|---|---|---|---|---|
| NMzi1 | 2 | 2 | 3 | 1 | 3 | 2.3 |
| NMzi1019 | 3 | 4 | 3 | 4 | 3 | 3.4 |
| NM26 | 4 | 2 | 3 | 1 | 5 | 3.2 |
| ZM4 | 3 | 5 | 3 | 3 | 2 | 3.3 |
| ZM5 | 3 | 5 | 3 | 5 | 3 | 3.7 |
| ZM8 | 4 | 4 | 3 | 5 | 3 | 3.7 |
| ZM10 | 2 | 1 | 3 | 1 | 3 | 2.1 |
| ZM11 | 3 | 2 | 3 | 3 | 3 | 2.8 |
| ZM12 | 2 | 3 | 3 | 4 | 3 | 2.9 |
| ZM168 | 5 | 4 | 4 | 5 | 2 | **4.0** |
| ZM09196 | 4 | 1 | 4 | 1 | 5 | 3.2 |

b

**Medium N (n = 27 plots, 11 varieties)**

| SN $m^{-2}$ | GW $m^{-2}$ | 3DCI | Can_Sur | Height | Overall rank |
|---|---|---|---|---|---|
| 1 | 5 | 1 | 5 | 3 | 2.8 |
| 3 | 2 | 3 | 2 | 3 | 2.7 |
| 4 | 3 | 5 | 4 | 4 | **4.0** |
| 3 | 3 | 3 | 3 | 3 | 3.0 |
| 3 | 4 | 4 | 5 | 2 | 3.5 |
| 4 | 3 | 4 | 1 | 2 | 3.1 |
| 2 | 5 | 1 | 4 | 3 | 3.0 |
| 3 | 2 | 3 | 2 | 3 | 2.7 |
| 1 | 3 | 1 | 3 | 3 | 2.1 |
| 4 | 3 | 3 | 5 | 3 | 3.5 |
| 5 | 2 | 5 | 1 | 4 | 3.7 |

c

**High N (n = 26 plots, 11 varieties)**

| SN $m^{-2}$ | GW $m^{-2}$ | 3DCI | Can_Sur | Height | Overall rank |
|---|---|---|---|---|---|
| 2 | 4 | 2 | 5 | 3 | 3.0 |
| 3 | 3 | 3 | 3 | 3 | 3.0 |
| 3 | 5 | 3 | 5 | 4 | **3.9** |
| 2 | 4 | 2 | 5 | 2 | 2.8 |
| 3 | 3 | 3 | 2 | 1 | 2.5 |
| 4 | 1 | 4 | 1 | 2 | 2.6 |
| 1 | 3 | 2 | 3 | 3 | 2.3 |
| 3 | 1 | 5 | 1 | 3 | 2.7 |
| 4 | 3 | 4 | 3 | 3 | 3.5 |
| 3 | 3 | 1 | 3 | 2 | 2.4 |
| 3 | 3 | 4 | 2 | 4 | 3.3 |

(**a-c**) A range of canopy measures (i.e. 3DCI and canopy surface area index), plot level height, and key yield components, i.e. spike number per metre square (SN $m^{-2}$) and grain number per metre square (GN $m^{-2}$), combined to assess winter wheat varieties under three N treatments, with 15% over the trimmed mean coloured dark orange, 7.5~15% coloured light orange, -7.5~7.5% coloured yellow, -15~-7.5% coloured light blue, and -15% below the trimmed mean coloured dark blue. Selected varieties were coloured red, indicating they were ranked higher than the other varieties by the performance matrix.

## Parsed Citations


**An N, Palmer CM, Baker RL, Markelz RJC, Ta J, Covington MF, Maloof JN, Welch SM, Weinig C (2016) Plant high-throughput phenotyping using photogrammetry and imaging techniques to measure leaf length and rosette area. Comput Electron Agric 127: 376–394**

Google Scholar: Author Only Title Only Author and Title

**Antonarakis AS, Richards KS, Brasington J, Muller E (2010) Determining leaf area index and leafy tree roughness using terrestrial laser scanning. Water Resour Res 46: 1–12**

Google Scholar: Author Only Title Only Author and Title

**Araus JL, Cairns JE (2014) Field high-throughput phenotyping: the new crop breeding frontier. Trends Plant Sci 19: 52–61**

Google Scholar: Author Only Title Only Author and Title

**Arnó J, Escolà A, Vallès JM, Llorens J, Sanz R, Masip J, Palacín J, Rosell-Polo JR (2013) Leaf area index estimation in vineyards using a ground-based LiDAR scanner. Precis Agric 14: 290–306**

Google Scholar: Author Only Title Only Author and Title

**Barker J, Zhang N, Sharon J, Steeves R, Wang X, Wei Y, Poland J (2016) Development of a field-based high-throughput mobile phenotyping platform. Comput Electron Agric 122: 74–85**

Google Scholar: Author Only Title Only Author and Title

**Bauer A, Bostrom AG, Ball J, Applegate C, Cheng T, Laycock S, Rojas SM, Kirwan J, Zhou J (2019) Combining computer vision and deep learning to enable ultra-scale aerial phenotyping and precision agriculture: A case study of lettuce production. Hortic Res 6: 1–12**

Google Scholar: Author Only Title Only Author and Title

**Bucksch A, Lindenbergh RC, Menenti M (2009) SkelTre-fast skeletonisation for imperfect point cloud data of botanic trees. In R Veltkamp, ed, Eurographics Work. 3D Object Retr. pp 1–8**

Google Scholar: Author Only Title Only Author and Title

**Burnette M, Rohde GS, Fahlgren N, Sagan V, Sidike P, Kooper R, Terstriep JA, Mockler T, Andrade-Sanchez P, Ward R, et al (2018) TERRA-REF data processing infrastructure. ACM IPEARC 18. ACM, Pittsburgh, pp 1–7**

Google Scholar: Author Only Title Only Author and Title

**Butler H, Chambers B, Hartzell P, Glennie C (2020) PDAL: An open source library for the processing and analysis of point clouds. Comput Geosci Dec: 104680**

Google Scholar: Author Only Title Only Author and Title

**Cabrera-Bosquet L, Fournier C, Brichet N, Welcker C, Suard BB, Tardieu F (2016) High-throughput estimation of incident light, light interception and radiation-use efficiency of thousands of plants in a phenotyping platform. New Phytol 212: 269–281**

Google Scholar: Author Only Title Only Author and Title

**Carpenter AE, Kamentsky L, Eliceiri KW (2012) A call for bioimaging software usability. Nat Methods 9: 666–70**

Google Scholar: Author Only Title Only Author and Title

**Cendrero-Mateo MP, Muller O, Albrecht H, Burkart A, Gatzke S, Janssen B, Keller B, Körber N, Kraska T, Matsubara S, et al (2017) Field Phenotyping: Challenges and Opportunities. Terr. Ecosyst. Res. Infrastructures. pp 53–80**

Google Scholar: Author Only Title Only Author and Title

**Cobb JN, DeClerck G, Greenberg A, Clark R, McCouch S (2013) Next-generation phenotyping: Requirements and strategies for enhancing our understanding of genotype-phenotype relationships and its relevance to crop improvement. Theor Appl Genet 126: 867–887**

Google Scholar: Author Only Title Only Author and Title

**Colmer J, O'Neill CM, Wells R, Bostrom A, Reynolds D, Websdale D, Shiralagi G, Lu W, Lou Q, Le Cornu T, et al (2020) SeedGerm: a cost-effective phenotyping platform for automated seed imaging and machine-learning based phenotypic analysis of crop seed germination. New Phytol 228: 778–793**

Google Scholar: Author Only Title Only Author and Title

**Cooley JW, Tukey JW (1965) An Algorithm for the Machine Calculation of Complex Fourier Series. Math Comput 19: 297**

Google Scholar: Author Only Title Only Author and Title

**Crain JL, Wei Y, Barker J, Thompson SM, Alderman PD, Reynolds M, Zhang N, Poland J (2016) Development and deployment of a portable field phenotyping platform. Crop Sci 56: 965–975**

Google Scholar: Author Only Title Only Author and Title

**Deery D, Jimenez-Berni J, Jones H, Sirault X, Furbank R (2014) Proximal Remote Sensing Buggies and Potential Applications for Field-Based Phenotyping. Agronomy 4: 349–379**

Google Scholar: Author Only Title Only Author and Title

**Deery DM, Rebetzke GJ, Jimenez-Berni JA, Condon AG, Smith DJ, Bechaz KM, Bovill WD (2020) Ground-Based LiDAR Improves Phenotypic Repeatability of Above-Ground Biomass and Crop Growth Rate in Wheat. Plant Phenomics 2020: 1–11**

Google Scholar: Author Only Title Only Author and Title

**Duan T, Chapman SC, Holland E, Rebetzke GJ, Guo Y, Zheng B (2016) Dynamic quantification of canopy structure to characterize early plant vigour in wheat genotypes. J Exp Bot 67: 4523–4534**
Google Scholar: Author Only Title Only Author and Title

**Duan T, Zheng B, Guo W, Ninomiya S, Guo Y, Chapman SC, A TD, A BZ, C WG, C SN, et al (2017) Comparison of ground cover estimates from experiment plots in cotton, sorghum and sugarcane based on images and ortho-mosaics captured by UAV. Funct Plant Biol 44: 169–183**
Google Scholar: Author Only Title Only Author and Title

**Duda RO, Hart PE (1972) Use of the Hough Transformation to Detect Lines and Curves in Pictures. Commun ACM 15: 11–15**
Google Scholar: Author Only Title Only Author and Title

**Edelsbrunner H, Kirkpatrick D, Seidel R (1983) On the shape of a set of points in the plane. IEEE Trans Inf theory 29: 551–559**
Google Scholar: Author Only Title Only Author and Title

**Feng W, Yao X, Zhu Y, Tian YC, Cao WX (2008) Monitoring leaf nitrogen status with hyperspectral reflectance in wheat. Eur J Agron 28: 394–404**
Google Scholar: Author Only Title Only Author and Title

**Fiorani F, Schurr U (2013) Future scenarios for plant phenotyping. Annu Rev Plant Biol 64: 267–91**
Google Scholar: Author Only Title Only Author and Title

**Firdousi R, Parveen S (2014) Local Thresholding Techniques in Image Binarization. Int J Eng Comput Sci 3: 4062–4065**
Google Scholar: Author Only Title Only Author and Title

**Friedli M, Kirchgessner N, Grieder C, Liebisch F, Mannale M, Walter A (2016) Terrestrial 3D laser scanning to track the increase in canopy height of both monocot and dicot crop species under field conditions. Plant Methods 12: 1–15**
Google Scholar: Author Only Title Only Author and Title

**Fritsche-Neto R, Borém A (2015) Phenomics: how next-generation phenotyping is revolutionazing plant breeding. doi: 10.1007/978-3-319-13677-6**
Google Scholar: Author Only Title Only Author and Title

**Furbank RT, Jimenez-Berni JA, George-Jaeggli B, Potgieter AB, Deery DM (2019) Field crop phenomics: enabling breeding for radiation use efficiency and biomass in cereal crops. New Phytol 223: 1714–1727**
Google Scholar: Author Only Title Only Author and Title

**Furbank RT, Tester M (2011) Phenomics - technologies to relieve the phenotyping bottleneck. Trends Plant Sci 16: 635–44**
Google Scholar: Author Only Title Only Author and Title

**Girardeau-Montaut D (2015) CloudCompare - User manual v2.6.1. Stuttgart, Germany**
Google Scholar: Author Only Title Only Author and Title

**Godwin RJ, Wood GA, Taylor JC, Knight SM, Welsh JP (2003) Precision farming of cereal crops: A review of a six year experiment to develop management guidelines. Biosyst Eng 84: 375–391**
Google Scholar: Author Only Title Only Author and Title

**Good AG, Shrawat AK, Muench DG (2004) Can less yield more? Is reducing nutrient input into the environment compatible with maintaining crop production? Trends Plant Sci 9: 597–605**

**Green CF., Dawkins TCK., Hunter B (1985) Influence of foliar applied chlormequat on radiation attenuation by winter barley canopies. J Agric Sci 105: 213–216**
Google Scholar: Author Only Title Only Author and Title

**Griffiths S, Simmonds J, Leverington M, Wang Y, Fish L, Sayers L, Alibert L, Orford S, Wingen L, Snape J (2012) Meta-QTL analysis of the genetic control of crop height in elite European winter wheat germplasm. Mol Breed 29: 159–171**
Google Scholar: Author Only Title Only Author and Title

**Griffiths S, Wingen L, Pietragalla J, Garcia G, Hasan A, Miralles D, Calderini DF, Ankleshwaria JB, Waite ML, Simmonds J, et al (2015) Genetic dissection of grain size and grain number trade-offs in CIMMYT wheat germplasm. PLoS One 10: 1–18**
Google Scholar: Author Only Title Only Author and Title

**Guo Q, Wu F, Pang S, Zhao X, Chen L, Liu J, Xue B, Xu G, Li L, Jing H, et al (2018) Crop 3D-a LiDAR based platform for 3D high-throughput crop phenotyping. Sci China Life Sci 61: 328–339**
Google Scholar: Author Only Title Only Author and Title

**Haralick R, Shanmugan K, Dinstein I (1973) Textural features for image classification. IEEE Trans Syst Man Cybern 3: 610–621**
Google Scholar: Author Only Title Only Author and Title

**Harkel J ten, Bartholomeus H, Kooistra L (2020) Biomass and Crop Height Estimation of Different Crops Using UAV-Based Lidar. Remote Sens 12: 1–18**
Google Scholar: Author Only Title Only Author and Title

**Hirafuji M, Yoichi H (2011) Creating high-performance/low-cost ambient sensor cloud system using OpenFS (Open Field Server) for high-throughput phenotyping. ... 2011 Proc. pp 2090–2092**
Google Scholar: Author Only Title Only Author and Title

**Holman FH, Riche AB, Castle M, Wooster MJ, Hawkesford MJ (2019) Radiometric Calibration of 'Commercial off the Shelf' Cameras for UAV-Based High-Resolution Temporal Crop Phenotyping of Reflectance and NDVI. Remote Sens 11: 1657**
Google Scholar: Author Only Title Only Author and Title

**Holman FH, Riche AB, Michalski A, Castle M, Wooster MJ, Hawkesford MJ (2016) High throughput field phenotyping of wheat plant height and growth rate in field plot trials using UAV based remote sensing. Remote Sens 8: 1–24**
Google Scholar: Author Only Title Only Author and Title

**Hosoi F, Omasa K (2009) Estimating vertical plant area density profile and growth parameters of a wheat canopy at different growth stages using three-dimensional portable lidar imaging. ISPRS J Photogramm Remote Sens 64: 151–158**
Google Scholar: Author Only Title Only Author and Title

**Howse J (2013) OpenCV Computer Vision with Python, 1st ed. Packt Publishing Ltd., Birmingham, UK**
Google Scholar: Author Only Title Only Author and Title

**Hyyppä E, Yu X, Kaartinen H, Hakala T, Kukko A, Vastaranta M, Hyyppä J (2020) Comparison of backpack, handheld, under-canopy UAV, and above-canopy UAV laser scanning for field reference data collection in boreal forests. Remote Sens 12: 1–31**
Google Scholar: Author Only Title Only Author and Title

**Jimenez-Berni JA, Deery DM, Rozas-Larraondo P, Condon ATG, Rebetzke GJ, James RA, Bovill WD, Furbank RT, Sirault XRR (2018) High throughput determination of plant height, ground cover, and above-ground biomass in wheat with LiDAR. Front Plant Sci 9: 1–18**
Google Scholar: Author Only Title Only Author and Title

**Jin S, Su Y, Wu F, Pang S, Gao S, Hu T, Liu J, Guo Q (2019) Stem-Leaf Segmentation and Phenotypic Trait Extraction of Individual Maize Using Terrestrial LiDAR Data. IEEE Trans Geosci Remote Sens 57: 1336–1346**
Google Scholar: Author Only Title Only Author and Title

**Jin S, Sun X, Wu F, Su Y, Li Y, Song S, Xu K, Ma Q, Baret F, Jiang D, et al (2021) Lidar sheds new light on plant phenomics for plant breeding and management: Recent advances and future prospects. ISPRS J Photogramm Remote Sens 171: 202–223**
Google Scholar: Author Only Title Only Author and Title

**Kachamba DJ, Ørka HO, Gobakken T, Eid T, Mwase W (2016) Biomass estimation using 3D data from unmanned aerial vehicle imagery in a tropical woodland. Remote Sens 8: 1–18**
Google Scholar: Author Only Title Only Author and Title

**Kelly D, Vatsa A, Mayham W, Ng L, Thompson A, Kazic T (2016) An opinion on imaging challenges in phenotyping field crops. Mach Vis Appl 27: 681–694**
Google Scholar: Author Only Title Only Author and Title

**Kirchgessner N, Liebisch F, Yu K, Pfeifer J, Friedli M, Hund A, Walter A (2017) The ETH field phenotyping platform FIP: A cable-suspended multi-sensor system. Funct Plant Biol 44: 154–168**
Google Scholar: Author Only Title Only Author and Title

**Korzeniowska K, Łącka M (2011) Generating dem from lidar data – comparison of available software tools. Arch Photogramm Cartogr Remote Sens 22: 271–284**
Google Scholar: Author Only Title Only Author and Title

**Kroon D-J (2009) NUMERICAL OPTIMIZATION OF KERNEL BASED IMAGE DERIVATIVES Dirk-Jan Kroon University of Twente , Enschede. Area**
Google Scholar: Author Only Title Only Author and Title

**Langer RHM, Liew FKY (1973) Effects of varying nitrogen supply at different stages of the reproductive phase on spikelet and grain production and on grain nitrogen in wheat. Aust J Agric Res 24: 647–656**
Google Scholar: Author Only Title Only Author and Title

**Li M, Shao MR, Zeng D, Ju T, Kellogg EA, Topp CN (2020a) Comprehensive 3D phenotyping reveals continuous morphological variation across genetically diverse sorghum inflorescences. New Phytol 226: 1873–1885**
Google Scholar: Author Only Title Only Author and Title

**Li P, Zhang X, Wang W, Zheng H, Yao X, Tian Y, Zhu Y, Cao W, Chen Q, Cheng T (2020b) Estimating aboveground and organ biomass of plant canopies across the entire season of rice growth with terrestrial laser scanning. Int J Appl Earth Obs Geoinf 91: 102132**
Google Scholar: Author Only Title Only Author and Title

**Li W, Niu Z, Huang N, Wang C, Gao S, Wu C (2015) Airborne LiDAR technique for estimating biomass components of maize: A case study in Zhangye City, Northwest China. Ecol Indic 57: 486–496**
Google Scholar: Author Only Title Only Author and Title

**Lin Y (2015) LiDAR: An important tool for next-generation phenotyping technology of high potential for plant phenomics? Comput Electron Agric 119: 61–73**

**Lindsay JB (2016) Whitebox GAT: A case study in geomorphometric analysis. Comput Geosci. doi: 10.1016/j.cageo.2016.07.003**
Google Scholar: Author Only Title Only Author and Title

**Lobet G (2017) Image Analysis in Plant Sciences: Publish Then Perish. Trends Plant Sci 22: 559–566**
Google Scholar: Author Only Title Only Author and Title

**Lowe DG (2004) Distinctive Image Features from Scale-Invariant Keypoints. Int J Comput Vis 60: 91–110**
Google Scholar: Author Only Title Only Author and Title

**Masiero A, Fissore F, Guarnieri A, Pirotti F, Visintini D, Vettore A (2018) Performance evaluation of two indoor mapping systems: Low-Cost UWB-aided photogrammetry and backpack laser scanning. Appl Sci 8: 1–19**
Google Scholar: Author Only Title Only Author and Title

**Mezirow J (1978) Perspective transformation. Adult Educ Q 28: 100–110**
Google Scholar: Author Only Title Only Author and Title

**Momen M, Campbell MT, Walia H, Morota G (2019) Predicting longitudinal traits derived from high-throughput phenomics in contrasting environments using genomic Legendre polynomials and B-splines. G3 Genes, Genomes, Genet 9: 3369–3380**
Google Scholar: Author Only Title Only Author and Title

**Naito H, Ogawa S, Valencia MO, Mohri H, Urano Y, Hosoi F, Shimizu Y, Chavez AL, Ishitani M, Selvaraj MG, et al (2017) Estimating rice yield related traits and quantitative trait loci analysis under different nitrogen treatments using a simple tower-based field phenotyping system with modified single-lens reflex cameras. ISPRS J Photogramm Remote Sens 125: 50–62**
Google Scholar: Author Only Title Only Author and Title

**Nguyen GN, Kant S (2018) Improving nitrogen use efficiency in plants: Effective phenotyping in conjunction with agronomic and genetic approaches. Funct Plant Biol 45: 606–619**
Google Scholar: Author Only Title Only Author and Title

**Omasa K, Hosoi F, Konishi A (2007) 3D lidar imaging for detecting and understanding plant responses and canopy structure. J Exp Bot 58: 881–898**
Google Scholar: Author Only Title Only Author and Title

**Panjvani K, Dinh A V., Wahid KA (2019) LiDARPheno – A low-cost LiDAR-based 3D scanning system for leaf morphological trait extraction. Front Plant Sci. doi: 10.3389/fpls.2019.00147**
Google Scholar: Author Only Title Only Author and Title

**Pask A, Pietragalla J, Mullan D, Reynolds M (2012) Physiological Breeding II: A Field Guide to Wheat Phenotyping. CIMMYT. doi: 10.1017/CBO9781107415324.004**
Google Scholar: Author Only Title Only Author and Title

**Paulus S (2019) Measuring crops in 3D: Using geometry for plant phenotyping. Plant Methods 15: 1–13**
Google Scholar: Author Only Title Only Author and Title

**Pieruschka R, Schurr U (2019) Plant Phenotyping: Past, Present, and Future. Plant Phenomics 2019: 1–6**
Google Scholar: Author Only Title Only Author and Title

**Power JF, Alessi J (1978) Tiller development and yield of standard and semidwarf spring wheat varieties as affected by nitrogen fertilizer. J Agric Sci 90: 97–108**
Google Scholar: Author Only Title Only Author and Title

**Powlson D, Norse D, Chadwick D, Lu Y, Zhang W, Zhang F (2014) Contribution of improved nitrogen fertilizer use to development of a low carbon economy in China. World Agric 4: 10–18**
Google Scholar: Author Only Title Only Author and Title

**Raun WR, Johnson GV (1999) Improving nitrogen use efficiency for cereal production. Agron J 91: 357–363**
Google Scholar: Author Only Title Only Author and Title

**Raybould A, Quemada H (2010) Bt crops and food security in developing countries: Realised benefits, sustainable use and lowering barriers to adoption. Food Secur 2: 247–259**
Google Scholar: Author Only Title Only Author and Title

**Reynolds D, Ball J, Bauer A, Davey R, Griffiths S, Zhou J (2019a) CropSight: A scalable and open-source information management system for distributed plant phenotyping and IoT-based crop management. Gigascience 8: 1–11**
Google Scholar: Author Only Title Only Author and Title

**Reynolds D, Baret F, Welcker C, Bostrom A, Ball J, Cellini F, Lorence A, Chawade A, Khafif M, Noshita K, et al (2019b) What is cost-efficient phenotyping? Optimizing costs for different scenarios. Plant Sci 282: 14–22**
Google Scholar: Author Only Title Only Author and Title

**Reynolds M, Langridge P (2016) Physiological breeding. Curr Opin Plant Biol 31: 162–171**
Google Scholar: Author Only Title Only Author and Title

**Ritter N, Ruth M (1997) The GeoTIFF data interchange standard for raster geographic images. Int J Remote Sens 18: 1637–1647**

Google Scholar: Author Only Title Only Author and Title

**Roitsch T, Cabrera-Bosquet L, Fournier A, Ghamkhar K, Jiménez-Berni J, Pinto F, Ober ES (2019) Review: New sensors and data-driven approaches-A path to next generation phenomics. Plant Sci 282: 2–10**
Google Scholar: Author Only Title Only Author and Title

**Roussel JR, Auty D, Coops NC, Tompalski P, Goodbody TRH, Meador AS, Bourdon JF, de Boissieu F, Achim A (2020) lidR: An R package for analysis of Airborne Laser Scanning (ALS) data. Remote Sens Environ 251: 112061**
Google Scholar: Author Only Title Only Author and Title

**Roy J, Tardieu F, Tixier-Boichard M, Schurr U (2017) European infrastructures for sustainable agriculture. Nat Plants 3: 756–758**
Google Scholar: Author Only Title Only Author and Title

**Sadras VO, Richards RA (2014) Improvement of crop yield in dry environments: Benchmarks, levels of organisation and the role of nitrogen. J Exp Bot 65: 1981–1995**
Google Scholar: Author Only Title Only Author and Title

**Sadras VO, Slafer GA (2012) Environmental modulation of yield components in cereals: Heritabilities reveal a hierarchy of phenotypic plasticities. F Crop Res 127: 215–224**
Google Scholar: Author Only Title Only Author and Title

**Sauvola J, Pietikäinen M (2000) Adaptive document image binarization. Pattern Recognit 33: 225–236**
Google Scholar: Author Only Title Only Author and Title

**Scharr H, Dee H, French AP, Tsaftaris SA (2016) Special issue on computer vision and image analysis in plant phenotyping. Mach Vis Appl 27: 607–609**
Google Scholar: Author Only Title Only Author and Title

**Shearman VJ, Scott RK, Foulkes MJ (2005) Crop Physiology and Metabolism. Physiological Processes Associated with Wheat Yield Progress in the UK. Crop Sci 185: 175–185**
Google Scholar: Author Only Title Only Author and Title

**Singh TR, Roy S, Singh OI, Sinam T, Singh KM (2012) A New Local Adaptive Thresholding Technique in Binarization. Int J Comput Sci Issues 8: 271–277**
Google Scholar: Author Only Title Only Author and Title

**Stovall AEL, Vorster AG, Anderson RS, Evangelista PH, Shugart HH (2017) Non-destructive aboveground biomass estimation of coniferous trees using terrestrial LiDAR. Remote Sens Environ 200: 31–42**
Google Scholar: Author Only Title Only Author and Title

**Su Y, Guo Q, Jin S, Guan H, Sun X, Ma Q, Hu T, Wang R, Li Y (2020) The Development and Evaluation of a Backpack LiDAR System for Accurate and Efficient Forest Inventory. IEEE Geosci Remote Sens Lett 1–5**
Google Scholar: Author Only Title Only Author and Title

**Su Y, Wu F, Ao Z, Jin S, Qin F, Liu B, Pang S, Liu L, Guo Q (2019) Evaluating maize phenotype dynamics under drought stress using terrestrial lidar. Plant Methods 15: 1–16**
Google Scholar: Author Only Title Only Author and Title

**Summerfield M (2015) Rapid GUI Programming with Python and Qt: The Definitive Guide to PyQt Programming. Pearson, London, UK**
Google Scholar: Author Only Title Only Author and Title

**Sun S, Li C, Paterson AH, Jiang Y, Xu R, Robertson JS, Snider JL, Chee PW (2018) In-field high throughput phenotyping and cotton plant growth analysis using LiDAR. Front Plant Sci 9: 1–17**
Google Scholar: Author Only Title Only Author and Title

**Susan S, Hanmandlu M (2013) A non-extensive entropy feature and its application to texture classification. Neurocomputing 120: 214–225**
Google Scholar: Author Only Title Only Author and Title

**Swarbreck SM, Wang M, Wang Y, Kindred D, Sylvester-Bradley R, Shi W, Varinderpal-Singh, Bentley AR, Griffiths H (2019) A Roadmap for Lowering Crop Nitrogen Requirement. Trends Plant Sci 24: 892–904**
Google Scholar: Author Only Title Only Author and Title

**Sylvester-Bradley R, Kindred DR (2009) Analysing nitrogen responses of cereals to prioritize routes to the improvement of nitrogen use efficiency. J Exp Bot 60: 1939–1951**
Google Scholar: Author Only Title Only Author and Title

**Tardieu F, Cabrera-Bosquet L, Pridmore T, Bennett M (2017) Plant Phenomics, From Sensors to Knowledge. Curr Biol 27: R770–R783**
Google Scholar: Author Only Title Only Author and Title

**Truong-Hong L, Laefer DF, Hinks T, Carr H (2013) Combining an angle criterion with voxelization and the flying voxel method in reconstructing building models from LiDAR data. Comput Civ Infrastruct Eng 28: 112–129**
Google Scholar: Author Only Title Only Author and Title

**Ubbens J, Cieslak M, Prusinkiewicz P, Stavness I (2018) The use of plant models in deep learning: An application to leaf counting in rosette plants. Plant Methods 14: 1–10**
Google Scholar: Author Only Title Only Author and Title

**UN Food & Agriculture Organization (2009) How to Feed the World in 2050. In FAO, ed, Proc. High-Level Expert Forum How to Feed World 2050. UN FAO, Rome, p 733**
Google Scholar: Author Only Title Only Author and Title

**Vadez V, Kholová J, Hummel G, Zhokhavets U, Gupta SK, Hash CT (2015) LeasyScan: A novel concept combining 3D imaging and lysimetry for high-throughput phenotyping of traits controlling plant water budget. J Exp Bot 66: 5581–5593**
Google Scholar: Author Only Title Only Author and Title

**Valluru R, Reynolds MP, Davies WJ, Sukumaran S (2017) Phenotypic and genome-wide association analysis of spike ethylene in diverse wheat genotypes under heat stress. New Phytol 214: 271–283**
Google Scholar: Author Only Title Only Author and Title

**Virlet N, Sabermanesh K, Sadeghi-Tehran P, Hawkesford MJ, Sabermanesh P, Sadeghitehran K, Hawkesford MJ, Sabermanesh K, Sadeghi-Tehran P, Hawkesford MJ (2017) Field Scanalyzer: An automated robotic field phenotyping platform for detailed crop monitoring. Funct Plant Biol 44: 143–153**
Google Scholar: Author Only Title Only Author and Title

**Virtanen P, Gommers R, Oliphant TE, Haberland M, Reddy T, Cournapeau D, Burovski E, Peterson P, Weckesser W, Bright J, et al (2020) SciPy 1.0: fundamental algorithms for scientific computing in Python. Nat Methods 17: 261–272**
Google Scholar: Author Only Title Only Author and Title

**Van Der Walt S, Colbert SC, Varoquaux G (2011) The NumPy array: A structure for efficient numerical computation. Comput Sci Eng 13: 22–30**
Google Scholar: Author Only Title Only Author and Title

**van der Walt S, Schönberger JL, Nunez-Iglesias J, Boulogne F, Warner JD, Yager N, Gouillart E, Yu T (2014) Scikit-image: image processing in Python. PeerJ 2: 1–18**
Google Scholar: Author Only Title Only Author and Title

**Walter JDC, Edwards J, McDonald G, Kuchel H (2019) Estimating Biomass and Canopy Height With LiDAR for Field Crop Breeding. Front Plant Sci. doi: 10.3389/fpls.2019.01145**
Google Scholar: Author Only Title Only Author and Title

**Wang C, Nie S, Xi X, Luo S, Sun X (2017) Estimating the biomass of maize with hyperspectral and LiDAR data. Remote Sens 9: 1–12**
Google Scholar: Author Only Title Only Author and Title

**Ward B, Brien C, Oakey H, Pearson A, Negrão S, Schilling RK, Taylor J, Jarvis D, Timmins A, Roy SJ, et al (2019) High-throughput 3D modelling to dissect the genetic control of leaf elongation in barley (Hordeum vulgare). Plant J 98: 555–570**
Google Scholar: Author Only Title Only Author and Title

**Wu D, Guo Z, Ye J, Feng H, Liu J, Chen G, Zheng J, Yan D, Yang X, Xiong X, et al (2019) Combining high-throughput micro-CT-RGB phenotyping and genome-wide association study to dissect the genetic architecture of tiller growth in rice. J Exp Bot 70: 545–561**
Google Scholar: Author Only Title Only Author and Title

**Yang W, Feng H, Zhang X, Zhang J, Doonan JH, Batchelor WD, Xiong L, Yan J (2020) Crop Phenomics and High-Throughput Phenotyping: Past Decades, Current Challenges, and Future Perspectives. Mol Plant 13: 187–214**
Google Scholar: Author Only Title Only Author and Title

**Zadocks JC, CHANG TT, KONZAK CF (1974) A decimal code for the growth stages of cereals. Weed Res 14: 415–421**
Google Scholar: Author Only Title Only Author and Title

**Zhang H, Li Y, Zhu JK (2018) Developing naturally stress-resistant crops for a sustainable agriculture. Nat Plants 4: 989–996**
Google Scholar: Author Only Title Only Author and Title

**Zhao C, Zhang Y, Du J, Guo X, Wen W, Gu S, Wang J, Fan J (2019) Crop phenomics: Current status and perspectives. Front Plant Sci. doi: 10.3389/fpls.2019.00714**
Google Scholar: Author Only Title Only Author and Title

**Zhao X, Guo Q, Su Y, Xue B (2016) Improved progressive TIN densification filtering algorithm for airborne LiDAR data in forested areas. ISPRS J Photogramm Remote Sens 117: 79–91**
Google Scholar: Author Only Title Only Author and Title

**Zhou J, Applegate C, Alonso AD, Reynolds D, Orford S, Mackiewicz M, Griffiths S, Penfield S, Pullen N (2017a) Leaf-GP: An open and automated software application for measuring growth phenotypes for arabidopsis and wheat. Plant Methods 13: 1–30**
Google Scholar: Author Only Title Only Author and Title

**Zhou J, Reynolds D, Websdale D, Le Cornu T, Gonzalez-Navarro O, Lister C, Orford S, Laycock S, Finlayson G, Stitt T, et al (2017b) CropQuant: An automated and scalable field phenotyping platform for crop monitoring and trait measurements to facilitate breeding and digital agriculture. bioRxiv 161547**
Google Scholar: Author Only Title Only Author and Title

**Zhou QY, Park J, Koltun V (2018) Open3D: A modern library for 3D data processing. arXiv 1–8**
Google Scholar: Author Only Title Only Author and Title